PRESENILIN 1 mutations causing early-onset familial Alzheimer's disease or familial acne inversa differ in their effects on genes facilitating energy metabolism and signal transduction

Karissa **Barthelson**[a*], Yang **Dong**[a], Morgan **Newman**[a] and Michael **Lardelli**[a]

[a] Alzheimer's Disease Genetics Laboratory, School of Biological Sciences, University of Adelaide, North Terrace, Adelaide, SA 5005, Australia

* Corresponding author

Complete correspondence address: Room 1.24, Molecular Life Sciences Building. North Terrace Campus. The University of Adelaide, SA 5005, Australia.

Telephone: 83134863

Email: karissa.barthelson@adelaide.edu.au

Running title: RNA-seq analysis of psen1 mutations

ABSTRACT

Background: The most common cause of early-onset familial Alzheimer's disease (EOfAD) is mutations in *PRESENILIN 1* (*PSEN1*) allowing production of mRNAs encoding full-length, but mutant, proteins. In contrast, a single known frameshift mutation in *PSEN1* causes familial acne inversa (fAI) without EOfAD. The molecular consequences of heterozygosity for these mutation types, and how they cause completely different diseases, remains largely unexplored.

Objective: To analyse brain transcriptomes of young adult zebrafish to identify similarities and differences in the effects of heterozygosity for *psen1* mutations causing EOfAD or fAI.

Methods: RNA sequencing was performed on mRNA isolated from the brains of a single family of 6-month-old zebrafish siblings either wild type or possessing a single, heterozygous EOfAD-like or fAI-like mutation in their endogenous *psen1* gene.

Results: Both mutations downregulate genes encoding ribosomal subunits, and upregulate genes involved in inflammation. Genes involved in energy metabolism appeared significantly affected only by the EOfAD-like mutation, while genes involved in Notch, Wnt and neurotrophin signalling pathways appeared significantly affected only by the fAI-like mutation. However, investigation of direct transcriptional targets of Notch signalling revealed possible increases in γ-secretase activity due to heterozygosity for either *psen1* mutation. Transcriptional adaptation due to the fAI-like frameshift mutation was evident.

Conclusion: We observed both similar and contrasting effects on brain transcriptomes of the heterozygous EOfAD-like and fAI-like mutations. The contrasting effects may illuminate how these mutation types cause distinct diseases.

KEY WORDS

Presenilin 1, RNA-seq, zebrafish, gamma-secretase, Alzheimer's disease, acne inversa

41 ## INTRODUCTION

42 Cases of Alzheimer's disease (AD) can be classified by age of onset and mode of inheritance.
43 Dominant mutations in a small number of genes cause AD with an age of onset younger than
44 65 years (early onset familial AD, EOfAD). On a population basis, around 60% of the
45 mutations causing EOfAD occur in one gene, *PRESENILIN 1* (*PSEN1*) [1-4].

46 *PSEN1* encodes a multi-pass transmembrane protein resident in the endoplasmic reticulum,
47 plasma membrane, endolysosomal pathway and other membranes [5, 6]. It has nine
48 recognised transmembrane domains [7]. A tenth transmembrane domain may exist when
49 PSEN1 protein is in its holoprotein state [7], before it undergoes autocatalytic
50 endoproteolysis to form the active catalytic core of γ-secretase [8], an enzyme complex
51 consisting of PSEN1 (or PSEN2), and the proteins NCSTN, PSENEN, and APH1A (or APH1B) [9,
52 10].

53 As a locus for genetic disease, *PSEN1* is truly remarkable both for the number of mutations
54 found there, and the variety of diseases these mutations cause. Mutations have been found
55 associated with Pick's disease [11], dilated cardiomyopathy [12] and acne inversa [13].
56 However, over 300 mutations of *PSEN1* are known to cause EOfAD
57 (www.alzforum.org/mutations/psen-1). In total, these mutations affect 161 codons of the
58 gene. Remarkably, the mutations are widely distributed in the PSEN1 coding sequence, but
59 are particularly common in the transmembrane domains. Only three regions of the PSEN1
60 protein are mostly devoid of EOfAD mutations: upstream of the first transmembrane

61 domain; a large part of the "cytosolic loop domain" (cytosolic loop 3); and the last two thirds
62 of the 9th transmembrane domain together with the lumenal C-terminus (see **Figure 1**).

63 The most common outcome of mutation of a protein sequence is either no effect or a
64 detrimental effect on the protein's evolved activity. Only rarely are mutations selectively
65 advantageous so that they enhance organismal survival and reproduction. The very large
66 number of EOfAD-causative mutations in *PSEN1* and their wide distribution in the protein
67 coding sequence is consistent with a loss-of-function. However, this cannot be a simple loss
68 of γ-secretase activity, as EOfAD-causative mutations have never been found in the genes
69 encoding the other components of γ-secretase complexes (other than less frequent
70 mutations in the *PSEN1* homologous gene, *PSEN2*, reviewed in [14]). Also, an *in vitro* analysis
71 of 138 EOfAD mutations of *PSEN1* published in 2017 by Sun et al. [15] found that
72 approximately 10% of these mutations actually increased γ-secretase activity.

73 Currently, the most commonly discussed hypothetical mechanism addressing how EOfAD
74 mutations of *PSEN1* cause disease is that these act through "qualitative changes" to γ-
75 secretase cleavage of the AMYLOID β A4 PRECURSOR PROTEIN (AβPP) to alter the length
76 distribution of the AMYLOID β (Aβ) peptides derived from it [16]. However, the
77 comprehensive study of Sun et al. revealed no consistency in the effects of *PSEN1* EOfAD
78 mutations on Aβ length distribution. The single consistent characteristic of all EOfAD
79 mutations in both *PSEN1* and *PSEN2* is that these permit production of transcripts with
80 coding sequences containing in-frame mutations, but terminated by the wild type stop
81 codons (i.e. they still permit production of a full length protein). This phenomenon was first
82 noted by De Strooper in 2007 [17] and described in detail by us in 2016 (the "reading frame

83 preservation rule" [18]). The universality of this rule, and that it reflects a critical feature of
84 the EOfAD-causative mechanism of *PSEN1* mutations, is shown by the fact that the
85 P242LfsX11 frameshift mutation of *PSEN1* (hereafter referred to as P242fs) causes a
86 completely different inherited disease, familial acne inversa (fAI, also known as hidradenitis
87 suppurativa), *without* EOfAD [13]. (Recently, a frameshift mutation in *PSEN1,* H21PfsX2, was
88 identified in an early-onset AD patient. However, whether the mutation is causative of
89 EOfAD mutation is still uncertain [19]. Questionable additional claims of EOfAD-causative
90 frameshift mutations in PSEN genes have been made and are reviewed in [18].) Critically, fAI
91 can also be caused by mutations in *NCSTN* and *PSENEN* [13], strongly supporting that this
92 disease is due to changes in γ-secretase activity.

93 Understanding the role of *PSENs* and their mutations is complicated by the partial functional
94 redundancy shared by *PSEN1* and *PSEN2* and their complex molecular biology. For example,
95 the PSEN1 holoprotein has been shown to have γ-secretase-independent activities required
96 for normal lysosomal acidification [20], can form multimers [21-24], and may interact with
97 the HIF1α protein [25-27] that is critical both for responses to hypoxia and for iron
98 homeostasis (reviewed in [28]). Additionally, within γ-secretase complexes, the PSENs act to
99 cleave at least 149 different substrates [29]. To simplify analysis, most previous investigation
100 of PSEN activity has involved inactivation (knock-out) of *PSEN1* and/or *PSEN2* in cells or
101 animals, and expression of only single forms of mutant PSEN (i.e. without simultaneous
102 expression of wild type forms). Forced expression of *PSEN* genes is also usually at non-
103 physiological levels which has unexpected regulatory feedback effects [30]. In humans,
104 investigating *PSEN*'s role in AD at the molecular level is restricted to post-mortem brain
105 tissues. However, these show substantially different patterns of gene expression compared

106 to the brains of people with mild cognitive impairment (MCI) or age-matched healthy
107 controls [31]. Since AD is thought to take decades to develop [32], we must understand the
108 pathological effects of EOfAD mutations in young adult brains if we wish to identify
109 preventative treatments. For this reason, we must model EOfAD mutations in animals.

110 The overwhelming majority of animal modelling of AD has utilised transgenic models
111 favoured for their apparent, partial reproduction of Aβ histopathology and easily discernible
112 cognitive disabilities. However, the relationship between Aβ histopathology and cognitive
113 change in these models is questionable [33]. Additionally, the most detailed form of
114 molecular phenotyping currently available, transcriptome analysis, shows little consistency
115 between the disturbed brain gene transcription of various transgenic models and limited
116 concordance between them and human sporadic AD brain transcriptomes [34]. "Knock-in"
117 mouse models of single EOfAD mutations (e.g. [35, 36]) make the fewest assumptions
118 regarding the pathological mechanism(s) of AD and most closely replicate the human EOfAD
119 genetic state (i.e. incorporating a single, dominant, endogenous mutation in the
120 heterozygous state). However, the brain transcriptomes of these mice have never been
121 analysed, and interest in them waned due to their lack of Aβ histopathology and mild
122 cognitive effects.

123 Analysis of mouse brain transcriptomes is complicated by strong effects on gene expression
124 of sex [37, 38] and, potentially, litter-of-origin (i.e. due to environmental and genotypic
125 variation) (K. Barthelson, unpublished results). In contrast, zebrafish brain transcriptomes
126 show only subtle influences of sex, and very large numbers of siblings can be generated from
127 single mating event, alleviating potential litter-of-origin issues [39-43]. In 2014, our

128 laboratory began a program of creating knock-in models of EOfAD-like (and non-EOfAD-like)
129 mutations in the zebrafish genes orthologous to *PSEN1*, *PSEN2*, and *SORL1*. In 2019 we
130 began publishing the results of transcriptome analyses of the young adult brains of these fish
131 [39-46] as we attempt to establish what effect(s) all the EOfAD mutations have in common
132 (and differentiate them from the non-EOfAD-like mutations).

133 Our previous analyses of an EOfAD-like mutation in the zebrafish *psen1* gene, Q96_K97del,
134 revealed very significant effects on the expression of genes involved in mitochondrial
135 function, lysosomal acidification, and iron homeostasis [45, 46]. Although Q96_K97del
136 follows the reading-frame preservation rule of EOfAD mutations in *PSEN1*, it is not an exact
137 equivalent of any human EOfAD-causative mutation. Consequently, in this study we aimed
138 to generate an additional, exactly equivalent, model of a human *PSEN1* EOfAD mutation. For
139 technical reasons, the T428 codon of zebrafish *psen1* (equivalent to the T440 codon of
140 human PSEN1) was predicted to be readily targetable using CRISPR-Cas9 technology, and we
141 subsequently deleted this codon in the zebrafish gene. This generated a zebrafish model of
142 the human EOfAD mutation $PSEN1^{T440del}$ [47]. This mutation was identified in a Japanese
143 man classified as displaying a mixed dementia phenotype (variant AD with spastic
144 paraparesis, Parkinson's disease and dementia with Lewy bodies). Also, to understand how
145 reading-frame preserving and frameshift mutations can cause completely different diseases
146 we generated a frameshift mutation in zebrafish *psen1*, $psen1^{W233fs}$, very similar to the fAI-
147 causative P242fs mutation of human *PSEN1*. We then performed an RNA-seq analysis with
148 high read depth and large sample numbers to compare the brain transcriptomes of fish from
149 a single family of young adult siblings heterozygous for either mutation or wild type. We
150 observed subtle, and mostly distinct, effects of the two mutations. In particular, changes in

151 the fAI-like brain transcriptomes implied significant effects on Notch, Wnt, neurotrophin,
152 and Toll-like receptor signalling, while changes in the EOfAD-like brain transcriptomes
153 implied effects on oxidative phosphorylation similar to those previously seen for EOfAD-like
154 mutations in *psen1* [45], *psen2* [40, 43], and *sorl1* [39, 41].

155 MATERIALS AND METHODS

156 *Zebrafish husbandry and animal ethics*

157 All zebrafish (Tübingen strain) used in this study were maintained in a recirculating water
158 system on a 14 hour light/10 hour dark cycle, fed dry food in the morning and live brine
159 shrimp in the afternoon. All zebrafish work was conducted under the auspices of the Animal
160 Ethics Committee (permit numbers S-2017-089 and S-2017-073) and the Institutional
161 Biosafety Committee of the University of Adelaide.

162 *CRISPR-Cas9 genome editing*

163 To mutate zebrafish *psen1,* we used the Alt-R® CRISPR-Cas9 system (Integrated DNA
164 Technologies, Coralville, IA, USA). To generate the T428del mutation (EOfAD-like) in exon 11
165 of *psen1*, we used a custom-designed crRNA recognising the sequence 5'
166 CTCCCCATCTCCATAACCTT 3' and a PAM of CGG. For the W233fs mutation (fAI-like), the
167 crRNA was designed to recognise the sequence 5' GATGAGCCATGCGGTCCACT 3' in exon 6
168 of *psen1,* with a PAM sequence of CGG. We aimed to generate exact equivalents of the
169 human P242fs mutation causing fAI, and the T440del mutation causing EOfAD by homology
170 directed repair (HDR). For the P242fs mutation, we used a plasmid DNA template as

171 described in [48] (synthesised by Biomatik, Kitchener, Ontario, Canada). For the T440del
172 mutation, we used an antisense, asymmetric single-stranded oligonucleotide with
173 phosphorothioate modifications (synthesised by Merck, Kenilworth, NJ, USA) as described in
174 [49] (HDR template DNA sequences are given in **Supplementary File 1.**)

175 Each crRNA was annealed with an equal amount of Alt-R® CRISPR-Cas9 tracrRNA (IDT) in
176 nuclease free duplex buffer (IDT) by heating at 95°C for 5 minutes, then allowed to cool to
177 room temperature, giving sgRNA solutions of 33 µM (assuming complete heteroduplex
178 formation of the RNA molecules). Then, 1 µL of the sgRNA solution was incubated with 1 µL
179 of Alt-R® S.p.Cas9 Nuclease 3NLS (IDT) at 64 µM at 37°C for 10 minutes to form
180 ribonucleoprotein (RNP) complexes. The final concentration for the linear ssODN for the
181 T428del mutation was 1 µM, and the final concentration of the plasmid DNA for the W233fs
182 mutation was 25 ng/µL. Approximately 2-5 nL of RNP complexes in solution with the
183 respective template DNAs were injected into Tübingen strain zebrafish embryos at the one
184 cell stage. The procedures followed for testing of the mutagenesis efficiencies of CRISPR-
185 Cas9 systems using allele-specific polymerase chain reactions and T7 endonuclease I assays,
186 and the breeding strategy to isolate the mutations of interest, are described in [41, 50].

187 *RNA-seq raw data generation and processing*

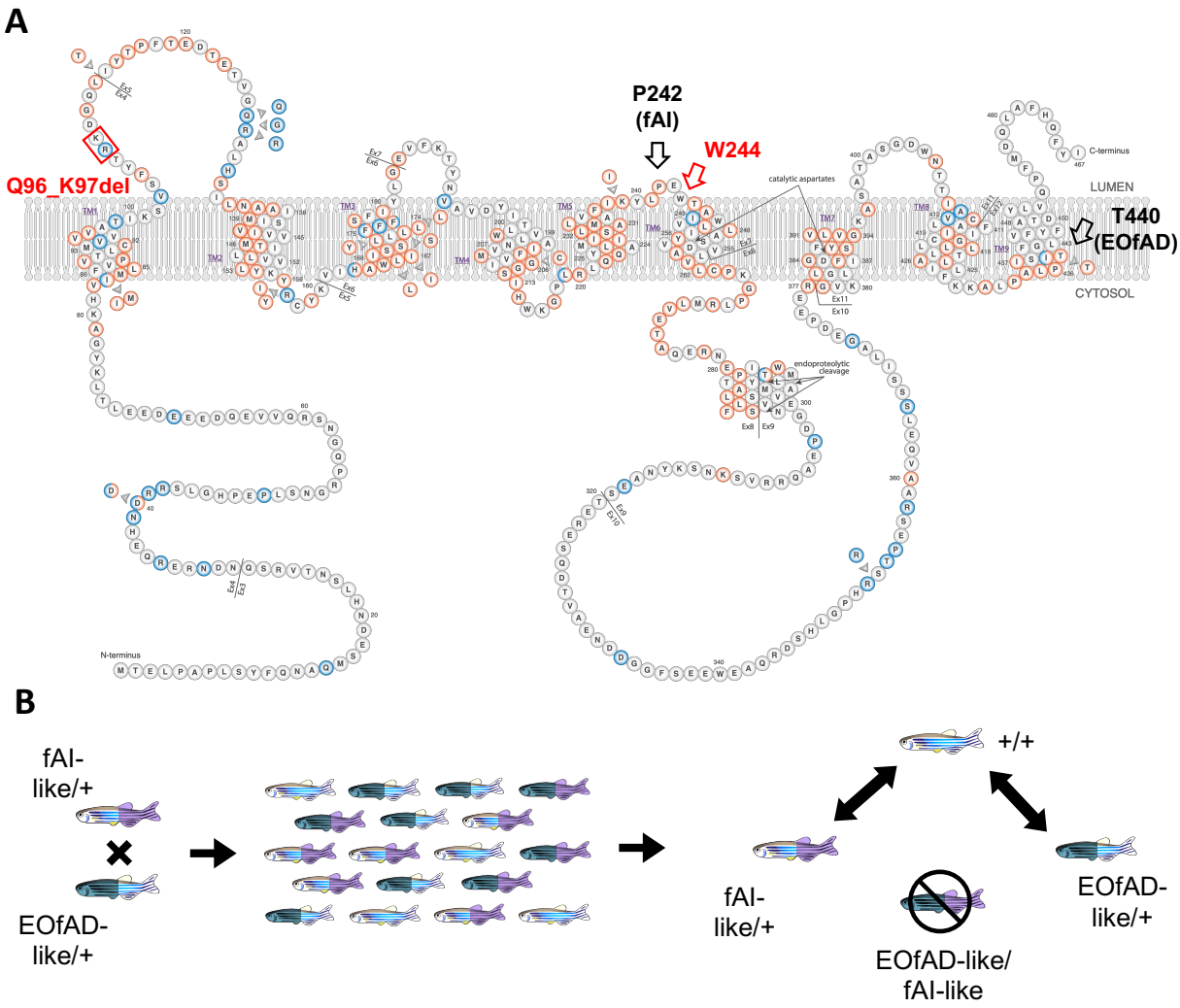

188

189 **Figure 1: Experimental design. A** Schematic of the human PSEN1 protein adapted from
190 https://www.alzforum.org/mutations/psen-1 with permission from FBRI LLC (Copyright © 1996–2020 FBRI LLC. All Rights
191 Reserved. Version 3.3 – 2020). Amino acid residues are colour-coded as to whether they are pathogenic for Alzheimer's
192 disease (red) or their pathogenicity is unclear (blue). The human mutation sites (P242 (fAI) and T440 (EOfAD) are indicated by
193 black arrows. The site of the zebrafish W233fs-equivalent codon (W244) is shown by the red arrow. Note that the human T440
194 codon is equivalent to the zebrafish T428 codon. The residues equivalent to those deleted in the Q96_K97del mutation of
195 zebrafish *psen1* analysed previously are indicated by a red box. **B** A fish heterozygous for the W233fs mutation (fAI-like/+) was
196 mated with a fish heterozygous for the T428del mutation (EOfAD-like/+). The resulting family of fish contain genotypes fAI-like/+,
197 EOfAD-like/+, EOfAD-like/fAI-like and their wild type siblings. The pairwise comparisons performed in the RNA-seq experiment
198 are depicted. Since the EOfAD-like/fAI-like genotype is not representative of any human disease, it was not analysed.

199 We performed RNA-seq on a family of zebrafish as described in **Figure 1**. Total RNA (with
200 genomic DNA depleted by DNaseI treatment) was isolated from the brains of n = 4 fish per
201 genotype and sex as described in [41]. Then, 500 ng of total RNA ($RIN_e > 9$) was delivered to
202 the South Australian Genomics Centre (SAGC, Adelaide, Australia) for polyA+ library
203 construction (with unique molecular identifiers (UMIs)) and RNA-sequencing using the
204 Illumina Novaseq S1 2x100 SE platform.

205 The raw fastq files from SAGC were provided as 100 bp paired end reads as well as an index
206 file containing the UMIs for each read (over two Novaseq lanes which were subsequently
207 merged). The merged raw data was processed using a developed Nextflow [51] RNA-seq
208 workflow (see https://github.com/sagc-bioinformatics/sagc-rnaseq-nf). Briefly, UMIs were
209 added to headers of each read using *fastp* (v0.20.1). Alignment of the reads to the zebrafish
210 genome (GRCz11, Ensembl release 98) was performed using *STAR* (v2.5.3a). Then, reads
211 which contained the same UMI (i.e. PCR duplicates) were deduplicated using the *dedup*
212 function of *umi_tools* (version 1.0.1). Finally, the gene-level counts matrix was generated
213 using *featureCounts* from the *Subread* (version 2.0.1) package.

214 *Differential gene expression*

215 Statistical analysis of the RNA-seq data was performed using *R* [52]. Since lowly expressed
216 genes are considered uninformative for differential expression analysis, we omitted genes
217 with less than 0.1 counts per million (CPM) (following the 10/minimum library size in millions
218 rule described in [53]). Library sizes after omitting the lowly expressed genes ranged
219 between 61 and 110 million reads. These were normalised using the trimmed mean of M-
220 values (TMM) method [54]. To test for differential expression of genes due to heterozygosity
221 for the T428del or W233fs mutation, we used a generalised linear model and likelihood ratio
222 tests using *edgeR* [55, 56]. A design matrix was specified with the wild type genotype as the
223 intercept, and the T428del/+ and W233fs/+ genotypes as the coefficients. We considered a
224 gene to be differentially expressed (DE) due to each *psen1* mutant genotype if the FDR
225 adjusted p-value was less than 0.05.

226 *Enrichment analysis*

227 We tested for over-representation of gene ontology (GO) terms within the DE gene lists
228 using *goseq* [57], using the average transcript length per gene to calculate the probability
229 weighting function (PWF). We considered a GO term to be significantly over-represented
230 within the DE gene lists relative to all detectable genes in the RNA-seq experiment if the
231 FDR-adjusted p-value generated by *goseq* was less than 0.05.

232 We also performed enrichment analysis on the entire list of detectable genes by calculating
233 the harmonic mean p-value from the raw p-values calculated from *fry* [58], *camera* [59] and
234 *fgsea* [60, 61] as described in [41]. To test for changes to gene expression in a broad range of

235 biological processes, we used the KEGG [62] gene sets obtained from MSigDB [63] using the
236 *msigdbr* package [64]. We also used *msigdbr* to obtain gene sets which contain genes that
237 show changed expression in response to changes in the Notch signalling pathway
238 (*NGUYEN_NOTCH1_TARGETS_UP* and *NGUYEN_NOTCH1_TARGETS_DN*, *NOTCH_DN.V1_UP*,
239 *NOTCH_DN.V1_DN* and *RYAN_MANTLE_CELL_LYMPHOMA_NOTCH_DIRECT_UP*). We also
240 tested for evidence of possible iron dyshomeostasis using gene sets containing genes
241 encoding transcripts which contain iron-responsive elements in their untranslated regions
242 (described in [45]).

243 *Comparison of the T428del and Q96_K97del mutations in psen1*

244 Isolation of the zebrafish Q96_K97del mutation in zebrafish *psen1* and analysis of its effects
245 on zebrafish brain transcriptomes have been described previously [45, 46]. That dataset is
246 comprised of brain RNA-seq data for fish heterozygous for the Q96_K97del mutation and
247 their wild type siblings, at 6 months old (young adult) and 24 months old (aged), and under
248 normoxia or hypoxia treatment (n = 4 fish per genotype, age and treatment). In the analysis
249 presented here, we performed enrichment analysis using the methods described above on
250 the entire dataset, but presented the results for the pairwise comparison between 6-month-
251 old Q96_K97del/+ fish and wild type fish under normoxia.

252 To obtain a broader comparison on the effects of the Q96_K97del and T428del mutations,
253 we performed adaptive, elastic-net sparse PCA (AES-PCA) [65] as implemented in the
254 *pathwayPCA* package [66]. For this analysis, we utilised the HALLMARK [67] gene sets from
255 MSigDB to generate the pathway collection. The pathway principal components (PCs) were

256 calculated only on the gene expression data from samples heterozygous for an EOfAD-like
257 mutation (Q96_K97del or T428del) and their wild type siblings under normoxia at 6 months
258 of age. Then, the categorical effect of genotype was tested for association with the pathway
259 PCs using a permutation-based regression model as described in [66].

260 *Data availability*

261 The paired end fastq files and the output of *featureCounts* have been deposited in GEO
262 under accession number GSE164466. Code to reproduce this analysis can be found at
263 https://github.com/karissa-b/psen1_EOfAD_fAI_6m_RNA-seq.

264 RESULTS

265 *Generation of an EOfAD-like and a fAI-like mutation in zebrafish psen1*

266 An unsolved puzzle regarding the dominant EOfAD mutations of human *PSEN1* (and *PSEN2*)
267 is why these are consistently found to permit production of transcripts in which the reading
268 frame is preserved, while heterozygosity for mutations causing frameshifts (or deleting the
269 genes) does not cause EOfAD. To investigate this quandary in an *in vivo* model, we initially
270 aimed to generate mutations in zebrafish *psen1* which would be exact equivalents of the
271 T440del and P242fs mutations using homology directed repair (HDR). While screening for
272 the desired mutations, we identified the mutations W233fs and T428del, both likely
273 generated by the non-homologous end joining (NHEJ) pathway of DNA repair. T428del is a 3
274 nucleotide deletion which, nevertheless, produces a protein-level change exactly equivalent
275 to that observed for the human T440del mutation. Hereafter, for simplicity, we refer to the

T428del mutation as “EOfAD-like”. W233fs is an indel mutation causing a frameshift in the second codon downstream of the zebrafish *psen1* proline codon equivalent to human *PSEN1* codon P242. This change is still within the short third lumenal loop of the Psen1 protein (see **Figure 1**). Assuming no effect on splicing, the frameshift mutation results in a premature stop codon 36 codons downstream of W233 (**Figure S1** in **Supplementary File 2**). Hereafter, we refer to this mutation as “fAI-like”. The alignment of the wild type and mutant sequences in humans and zebrafish is shown in **Figure 2**.

Heterozygosity or homozygosity for neither the EOfAD-like nor the fAI-like mutation produces any obvious morphological defects. However, this is unsurprising considering that rare examples of humans homozygous for EOfAD mutations are known [68, 69] and loss of *PSEN1* γ-secretase activity is, apparently, compatible with viability in zebrafish [70] and rats [71] (although not in mice [72]).

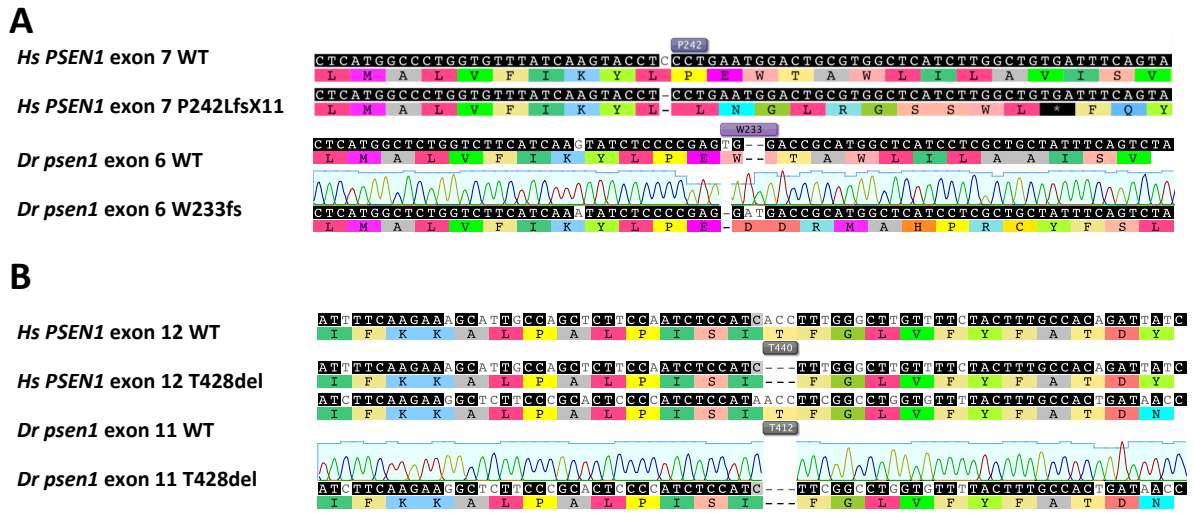

289 **Figure 2: A** Alignment of a region of wild type human (*Hs*) *PSEN1* exon 7, and the same region containing the human P242fs
290 (P242LfsX11) mutation, and the equivalent zebrafish (*Dr*) *psen1* exon 6 wild type and W233fs sequences. **B** Alignment of a
291 region of wild type human (*Hs*) *PSEN1* exon 12, and the same region containing the human T440del mutation, and the
292 equivalent zebrafish (*Dr*) *psen1* exon 11 wild type and T428del sequences.

293 *Transcriptome analysis*

294 To investigate global changes to the brain transcriptome due to heterozygosity for the
295 EOfAD-like or fAI-like mutations in *psen1,* we performed mRNA-seq on a family of fish as
296 described in **Figure 1**. The family of sibling fish were raised together in a single tank, thereby
297 reducing sources genetic and environmental variation between individuals and allowing
298 subtle changes to the transcriptome to be detected with minimal confounding effects.

299 To begin our exploration of the similarities and differences between the brain
300 transcriptomes of the mutant and wild type fish, we first performed principal component
301 analysis (PCA) on the gene level, log transformed counts per million (logCPM) of the
302 zebrafish RNA-seq samples. A plot of principal component 1 (PC1) against PC2 did not show
303 distinct clustering of samples by genotype or sex, indicating that these variables do not
304 result in stark changes to the brain transcriptome. This is consistent with our previous
305 observations of EOfAD-like mutations in other genes [39-41]. However, some separation of
306 the EOfAD-like and fAI-like samples is observed across PC2, indicating distinct, but subtle,
307 differences between these transcriptomes. Notably, the majority of the variation in this
308 dataset is not captured until PC6 (**Figure 3**).

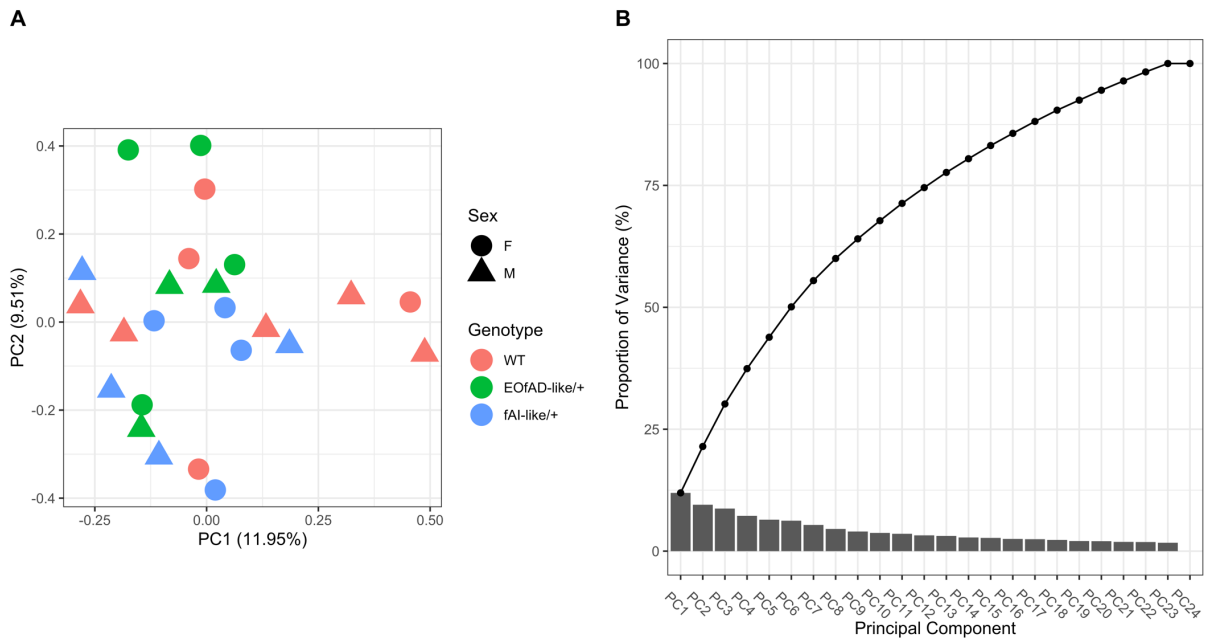

309

310 **Figure 3:** Principal component (PC) analysis of the gene expression values for the RNA-seq experiment. **A** PC1 plotted against
311 PC2 for each sample. Each point represents a sample and is coloured according to *psen1* genotype. Female (F) samples
312 appear as circles and male (M) samples appear as triangles. **B** Scree plot indicating the variance explained by each principal
313 component. The points joined by lines indicate the cumulative variance explained by each PC.

314 *Heterozygosity for the EOfAD-like or fAI-like mutations of psen1 causes only subtle effects on*
315 *gene expression*

316 Which genes are dysregulated due to heterozygosity for the EOfAD-like or the fAI-like
317 mutations? To address this question, we performed differential gene expression analysis
318 using a generalised linear model and likelihood ratio tests with *edgeR*. We observed
319 statistical evidence for 13 genes as significantly differentially expressed (DE) due to
320 heterozygosity for the EOfAD-like mutation, and 5 genes due to the fAI-like mutation (**Figure**
321 **4**, **Supplementary Table 1**). Notably, *psen1* was the most significantly DE gene due to
322 heterozygosity for the fAI-like mutation (logFC = -0.8, FDR = 1.33e-78), consistent with the

323 observation that frame-shift mutations commonly induce nonsense-mediated mRNA decay
324 when they result in premature stop codons (reviewed in [73]). Total levels of *psen1*
325 transcripts were unchanged in EOfAD-like/+ brains (logFC = -0.0065, FDR = 1, **Figure S7** in
326 **Supplementary File 2**). No DE genes were found to be shared between the comparisons of
327 either form of heterozygous mutant to wild type, or were found to be significantly
328 overrepresented by any gene ontology (GO) terms by *goseq* (for the top 5 most significantly
329 over-represented GO terms in each comparison, see **Tables S1** and **S2** in **Supplementary File**
330 **2**). This is not unexpected due to the relatively low number of significantly DE genes
331 detected.

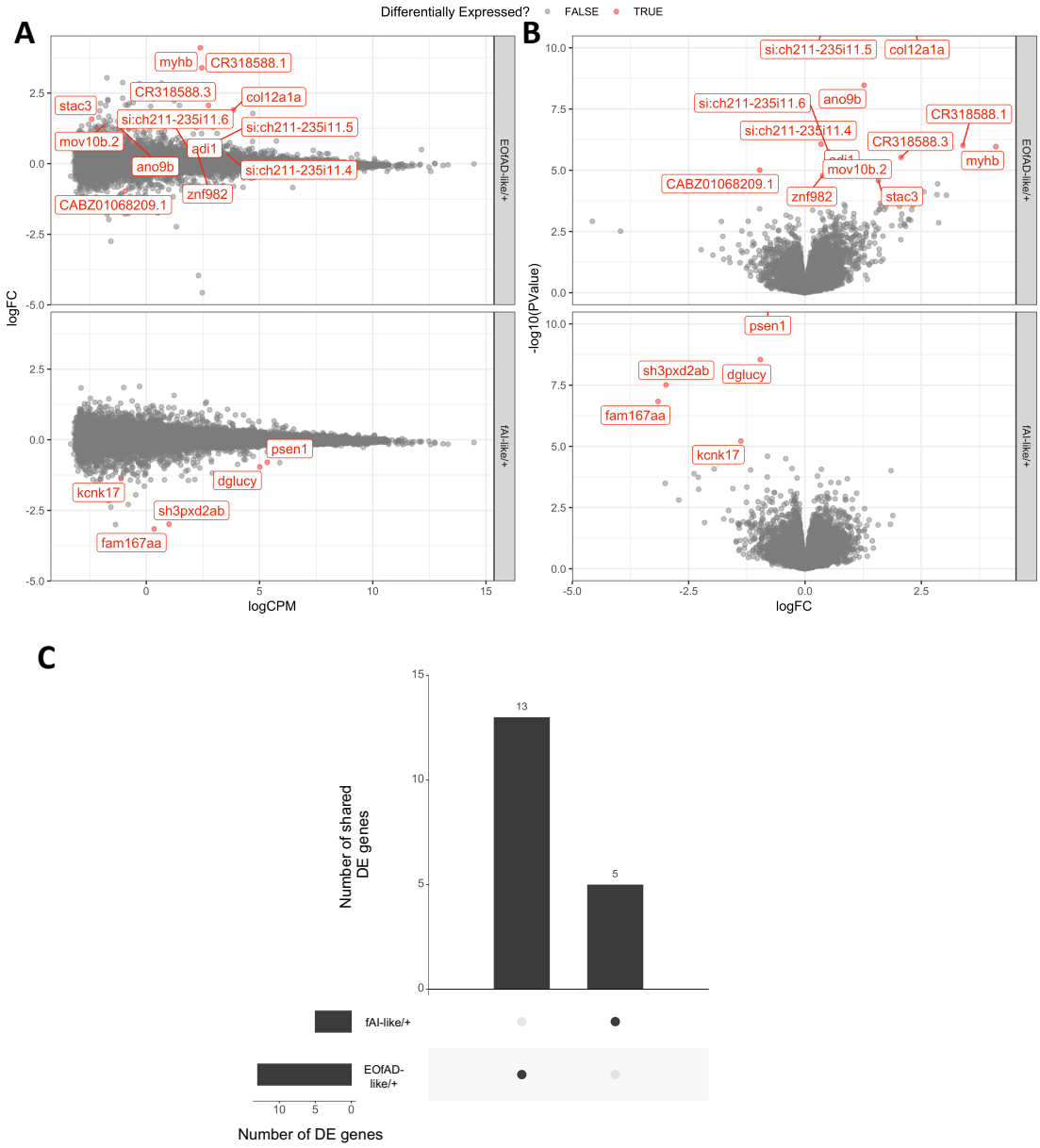

Figure 4: Differential expression analysis. **A** Mean-difference (MD) plots and **B** volcano plots of changes to gene expression in EOfAD-like/+ and fAI-like/+ mutant zebrafish brains. Note that the limits of the y-axis in **B** are restrained to between 0 and 10 for visualisation purposes. **C** Upset plot indicating the low number of genes which are significantly differentially expressed (DE) in either comparison.

337 *Significant differences in gene expression between the EOfAD-like and fAI-like mutants can be*
338 *detected at the pathway level.*

339 Since very few DE genes were detected in each comparison of heterozygous *psen1* mutant
340 fish to their wild type siblings, we performed enrichment analysis on all detectable genes in
341 the RNA-seq experiment. Our method, inspired by the *EGSEA* framework [74], involves
342 calculation of the harmonic mean p-value [75] from the raw p-values of three different rank-
343 based gene set testing methods: *fry* [58], *camera* [59] and *GSEA* [60, 61]. Unlike *EGSEA*, we
344 use the harmonic mean p-value to combine the raw p-values, as the harmonic mean p-value
345 has been specifically shown to be robust for combining dependent p-values [75]. We
346 performed enrichment testing using the KEGG gene sets (describing 186 biological pathways
347 and processes) to obtain information on changes to activities for these pathways. We also
348 tested for evidence of iron dyshomeostasis using our recently defined sets of genes
349 containing iron-responsive elements (IREs) in the untranslated regions of their mRNAs [45].
350 We observed statistical evidence for 7 KEGG gene sets as significantly altered by
351 heterozygosity for the EOfAD-like mutation and 11 KEGG gene sets as significantly altered by
352 heterozygosity for the fAI-like mutation (**Figure 5,** full results of the raw p-values from each
353 algorithm as well as the harmonic mean p-value can be found in **Supplementary Table 2**).
354 Gene sets significantly altered in the brains of both forms of heterozygous mutant included
355 the KEGG gene sets for cytokine receptor interactions, Jak/Stat signalling, and encoding the
356 components of the ribosomal subunits. Inspection of the leading edge genes (which can be
357 interpreted as the core genes driving the enrichment of a gene set) showed that similar
358 genes were driving the enrichment of the gene sets for cytokine receptor interactions and
359 Jak/Stat signalling. Similar genes were also driving the enrichment of the *KEGG_RIBOSOME*

360 gene set in both heterozygous mutants. However, the magnitude of the logFC was greater in
361 the fAI-like/+ samples, suggesting a stronger effect (**Figure S4-S6** in **Supplementary File 2**).
362 Gene sets which were only altered significantly by heterozygosity for the EOfAD-like
363 mutation were involved in energy metabolism (*KEGG_PARKINSONS_DISEASE*,
364 *KEGG_OXIDATIVE_PHOSPHORYLATION*, *and KEGG_CITRATE_CYCLE_TCA_CYCLE*). Notably,
365 the KEGG gene sets for Parkinson's disease, Huntington's disease, and for oxidative
366 phosphorylation, share 55 leading-edge genes, implying that their enrichment is driven by,
367 essentially, the same gene expression signal (**Figure 5**). Conversely, the 10 KEGG gene sets
368 found to be altered significantly by heterozygosity for the fAI-like mutation appear to be
369 driven mostly by distinct gene expression signals. No IRE gene sets were observed
370 statistically to be altered in the brains of either mutant, suggesting that iron homeostasis is
371 unaffected (at least at 6 months of age). The changes to expression of genes within the KEGG
372 gene sets are likely not due to broad changes in cell-type proportions in the zebrafish brain
373 samples, since the expression of marker genes of neurons, astrocytes, oligodendrocytes and
374 microglia was similar in all samples (**Figure S13** in **Supplementary File 2**).

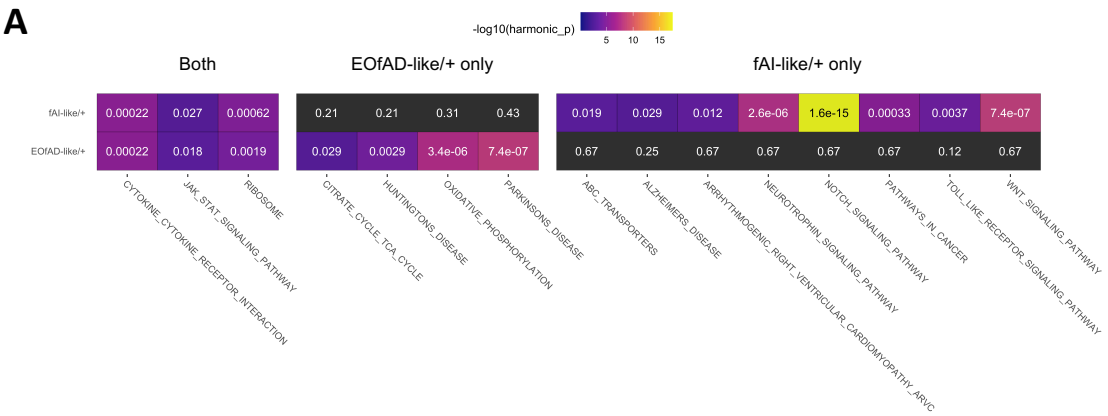
A
-log10(harmonic_p)
5
10
15
Both
EOfAD-like/+ only
fAI-like/+ only
fAI-like/+
EOfAD-like/+
0.00022
0.027
0.00062
0.00022
0.018
0.0019
0.21
0.21
0.31
0.43
0.029
0.0029
3.4e-06
7.4e-07
0.019
0.029
0.012
2.6e-06
1.6e-15
0.00033
0.0037
7.4e-07
0.67
0.25
0.67
0.67
0.67
0.67
0.12
0.67
CYTOKINE_CYTOKINE_RECEPTOR_INTERACTION
JAK_STAT_SIGNALING_PATHWAY
RIBOSOME
CITRATE_CYCLE_TCA_CYCLE
HUNTINGTONS_DISEASE
OXIDATIVE_PHOSPHORYLATION
PARKINSONS_DISEASE
ABC_TRANSPORTERS
ALZHEIMERS_DISEASE
ARRHYTHMOGENIC_RIGHT_VENTRICULAR_CARDIOMYOPATHY_ARVC
NEUROTROPHIN_SIGNALING_PATHWAY
NOTCH_SIGNALING_PATHWAY
PATHWAYS_IN_CANCER
TOLL_LIKE_RECEPTOR_SIGNALING_PATHWAY
WNT_SIGNALING_PATHWAY

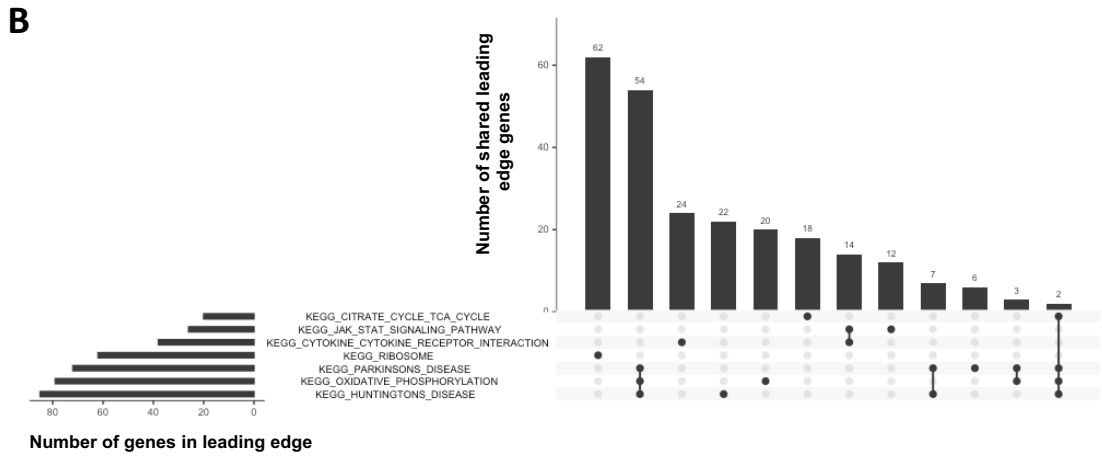
B
Number of shared leading edge genes
62
54
24
22
20
18
14
12
7
6
3
2
KEGG_CITRATE_CYCLE_TCA_CYCLE
KEGG_JAK_STAT_SIGNALING_PATHWAY
KEGG_CYTOKINE_CYTOKINE_RECEPTOR_INTERACTION
KEGG_RIBOSOME
KEGG_PARKINSONS_DISEASE
KEGG_OXIDATIVE_PHOSPHORYLATION
KEGG_HUNTINGTONS_DISEASE
Number of genes in leading edge

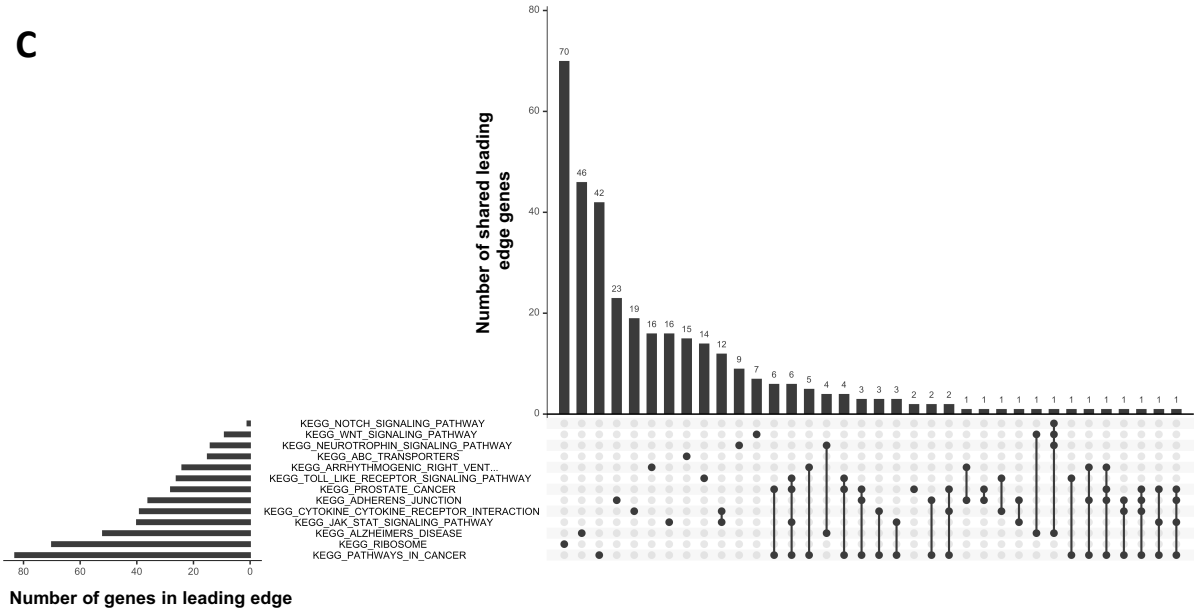
C
Number of shared leading edge genes
70
46
42
23
19
16
16
15
14
12
9
7
6
6
5
4
4
3
3
3
2
2
2
KEGG_NOTCH_SIGNALING_PATHWAY
KEGG_WNT_SIGNALING_PATHWAY
KEGG_NEUROTROPHIN_SIGNALING_PATHWAY
KEGG_ABC_TRANSPORTERS
KEGG_ARRHYTHMOGENIC_RIGHT_VENT...
KEGG_TOLL_LIKE_RECEPTOR_SIGNALING_PATHWAY
KEGG_PROSTATE_CANCER
KEGG_ADHERENS_JUNCTION
KEGG_CYTOKINE_CYTOKINE_RECEPTOR_INTERACTION
KEGG_JAK_STAT_SIGNALING_PATHWAY
KEGG_ALZHEIMERS_DISEASE
KEGG_RIBOSOME
KEGG_PATHWAYS_IN_CANCER
Number of genes in leading edge

375

376 **Figure 5: A** KEGG gene sets with FDR-adjusted harmonic mean p-values of < 0.05 in *psen1* EOfAD-like/+ and fAI-like/+ mutant
377 brains. The colour of the cells indicates the level of significance (brighter colour indicates greater statistical significance, while
378 dark grey indicates the FDR-adjusted harmonic mean p-value > 0.05). The number within each cell is the FDR-adjusted
379 harmonic mean p-value. **B** Upset plot indicating the overlap of leading edge genes from the fgsea algorithm which drive the
380 enrichment of gene sets significantly altered in EOfAD-like/+ and **C** fAI-like/+ brains.

381 ### *The EOfAD-like and fAI-like mutations alter expression of Notch signalling genes*

382 Notch signalling plays a critical role in many cell differentiation events and is dependent on
383 PSEN's γ-secretase activity. Disturbance of Notch signalling due to decreased γ-secretase
384 activity has been suggested to contribute to the changes in skin histology of fAI, as Notch
385 signalling is required for normal epidermal maintenance ([76-78] and reviewed by [79]).
386 However, fAI has not been reported as associated with EOfAD, despite that the T440del
387 mutant form of *PSEN1* appears to have little intrinsic γ-secretase activity [15]. The expression
388 of genes involved in the KEGG gene set for the Notch signalling pathway was observed to be
389 highly significantly altered in the brains of fAI-like/+ mutants, but not of EOfAD/+ mutants,
390 implying that γ-secretase activity might only be affected significantly by the frameshift, fAI-
391 like mutation (**Figure 5**). However, inspection of the logFC of genes in the
392 *KEGG_NOTCH_SIGNALING_PATHWAY* gene set revealed similar patterns of changes to gene
393 expression in both mutants (**Figure 6**). Upregulation of the genes encoding the Notch and
394 Delta receptors is observed in both mutants compared to wild type. In fAI-like/+ brains, we
395 observe downregulation of the downstream transcriptional targets of the Notch intracellular
396 domain (NICD), implying decreased Notch signalling (and, likely, reduced γ-secretase
397 activity). Genes encoding repressors of Notch signalling are observed to be upregulated (i.e.
398 *dyl* and *numb*), reinforcing this interpretation.

399 Since the KEGG gene set for Notch signalling only contains two genes that are direct
400 transcriptional targets of the NICD, we investigated further whether Notch signalling is
401 perturbed in both mutants by analysis of gene sets from MSigDB containing information on
402 genes responsive to Notch signalling in different cell lines: *NGUYEN_NOTCH1_TARGETS_UP*;
403 *NGUYEN_NOTCH1_TARGETS_DN*; *NOTCH_DN.V1_UP*; *NOTCH_DN.V1_DN*; and
404 *RYAN_MANTLE_CELL_LYMPHOMA_NOTCH_DIRECT_UP*. The
405 *NGUYEN_NOTCH1_TARGETS_UP* and *_DOWN* gene sets consist of genes which have been
406 observed as up- or downregulated respectively in response to a constitutively active Notch
407 receptor in keratinocytes [80]. *The NOTCH_DN.V1_UP* and *_DN* gene sets contain genes
408 which are up- and down-regulated respectively in response to treatment with the γ-
409 secretase inhibitor DAPT in a T-cell acute lymphoblastic leukemia (T-ALL) cell line [81]. The
410 *RYAN_MANTLE_CELL_LYMPHOMA_NOTCH_DIRECT_UP* gene set contains genes showing
411 both increased expression upon rapid activation of Notch signalling by washout of the γ-
412 secretase inhibitor compound E, and evidence for a NICD binding site in the promotor by
413 ChIP-seq, in mantle cell lymphoma cell lines [82]. (Note that there is no equivalent
414 "*RYAN_MANTLE_CELL_LYMPHOMA*" gene set representing genes downregulated in
415 response to Notch signalling.) Of these 5 gene sets, statistical support was found only for
416 changes to the expression of genes in the
417 *RYAN_MANTLE_CELL_LYMPHOMA_NOTCH_DIRECT_UP* gene set, and this was found for
418 both the EOfAD-like (p=0.006) and the fAI-like (p=0.008) mutants. The leading edge genes
419 were mostly observed to be upregulated, which supports increases in Notch signalling
420 (implying increased γ-secretase activity). Transcriptional adaptation (previously known as
421 "genetic compensation") might contribute to the apparent increase in Notch signalling in the
422 frameshift, fAI-like/+ mutant brains via upregulated expression of the *psen1*-homologous

423 gene, *psen2* [83, 84]. Although no statistically significant differences in expression were
424 observed for *psen2* in the differential expression test using *edgeR* (see **Supplementary Table**
425 **1**), a trend towards upregulation in the fAI-like/+ mutants was observed following a simple
426 Student's t-test (p=0.074, **Figure 6D**). El-Brolosy et al. [83] showed that the wild type allele of
427 a mutated gene can also be upregulated by transcriptional adaptation (where the mutation
428 causes nonsense-medicated decay, NMD, of mutant transcripts). Inspection of the number
429 of reads aligning to the W233 mutation site across samples indicates that the expression of
430 the wild type *psen1* allele in fAI-like/+ brains appears to be greater than 50% of the
431 expression of the wild type *psen1* allele in wild type brains (p = 0.006), providing further
432 evidence for transcriptional adaptation due to the fAI-like mutation (**Figure S8** in
433 **Supplementary File 2**).

434 Together, these results suggest that Notch signalling and, by implication, γ-secretase activity,
435 may be enhanced in *psen1* mutant brains. However, future biochemical assays should be
436 performed to confirm this prediction.

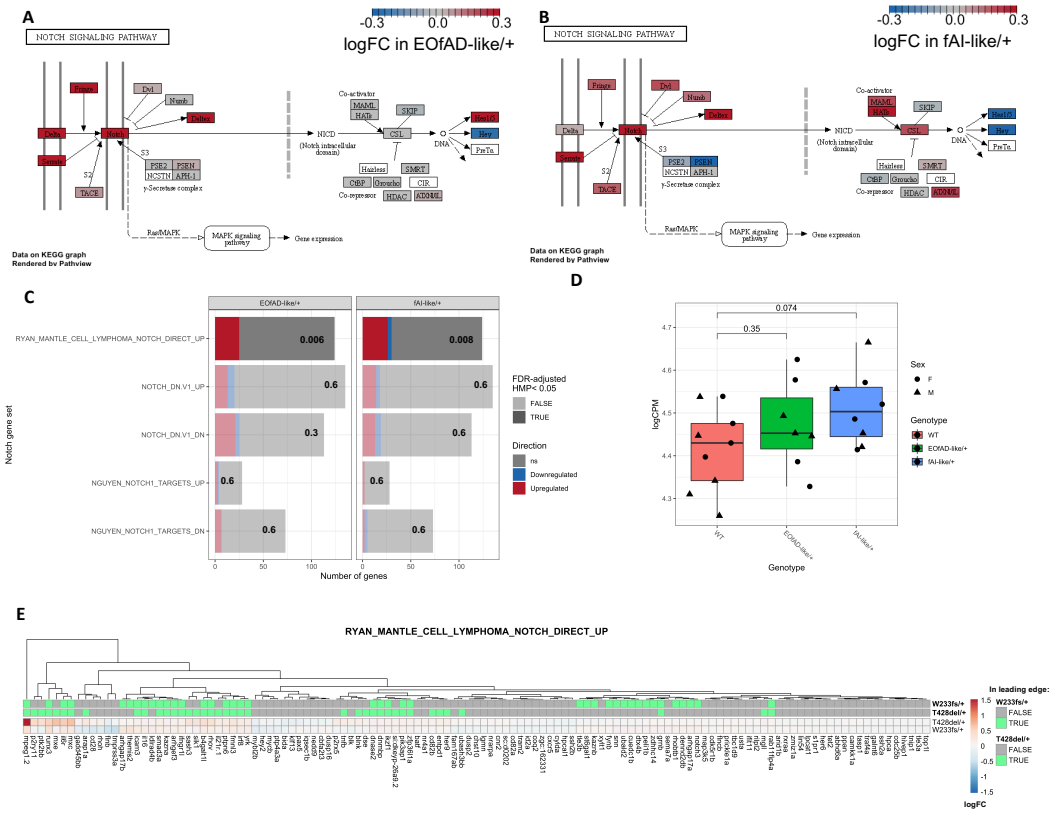

Figure 6: A Pathview [85] visualisation of the changes to gene expression in the *KEGG_NOTCH_SIGNALING_PATHWAY* gene set in EOfAD-like/+ mutants and **B** fAI-like/+ mutants. **C** The proportion of genes with increased expression (red, z > √2) and decreased expression (blue, z < √2) in MSigDB gene sets for Notch signalling in EOfAD-like/+ and fAI-like/+ mutant brains. Gene sets which contained a FDR-adjusted harmonic mean p-value (HMP) < 0.05 appear less transparent. The FDR adjust p-values are also listed on the bars. **D** The expression of *psen2* is trending towards upregulation, particularly in fAI-like/+ mutants. Here, p-values were determined by Student's unpaired t-tests. **E** Heatmap indicating the logFC values for genes in the *RYAN_MANTLE_CELL_LYMPHOMA_NOTCH_DIRECT_UP* gene set. Genes are clustered based on their Euclidean distance, and are labelled with green if they appear in the leading edge of the *fgsea* algorithm for each comparison of a *psen1* heterozygous mutant with wild type.

The EOfAD-like mutation T428del has a milder phenotype than the previously studied Q96_K97del EOfAD-like mutation of psen1

The T428del mutation of *psen1* is the first identified zebrafish mutation exactly equivalent, (at the protein sequence level), to a characterised human EOfAD mutation. Therefore, we

451 sought to assess the consistency of its effects with those of a previously studied EOfAD-like
452 mutation, Q96_K97del, and to identify cellular processes affected in common by the two
453 mutations. The Q96_K97del mutation deletes two codons in the sequence encoding the first
454 lumenal loop of the Psen1 protein (see **Figure 1**). Comparison of transcriptomes from the 6-
455 month-old brains of Q96_K97del/+ and wild type siblings previously predicted changes to
456 expression of genes involved in energy metabolism, iron homeostasis and lysosomal
457 acidification [45, 46]. To compare which cellular processes are affected by heterozygosity for
458 the Q96_K97del mutation or the T428del mutation, we first performed enrichment analysis
459 on the RNA-seq data previously generated by our analysis of zebrafish heterozygous for the
460 Q96_K97del mutation relative to their wild type siblings. Here, we observed that
461 heterozygosity for the Q96_K97del mutation results in significant alterations in 7 KEGG gene
462 sets (at 6 months of age during normoxia, Figure 7A). We also found statistical evidence for
463 altered expression of genes possessing IREs in their 3' UTRs (see *IRE3_ALL* in **Figure 7A**),
464 consistent with our previous finding using a different method of enrichment analysis [45].
465 Gene sets affected in common between the two EOfAD-like mutations in *psen1* are involved
466 in energy metabolism and protein translation (**Figure 7A**). The expression of genes involved
467 in protein degradation, and of genes containing IREs in the 3' UTRs of their transcripts,
468 appeared significantly altered only by the Q96_K97del mutation (**Figure 7A**).

469 We also compared the effects of the two EOfAD-like mutations using adaptive, elastic-net
470 sparse PCA (AES-PCA) as implemented in the *pathwayPCA* package [66]. AES-PCA allows
471 reduction of data dimensionality and for the overall activity of predefined gene sets to be
472 observed in a sample-specific manner [65]. To obtain a global view of the changes to gene
473 expression between the two *psen1* EOfAD-like mutations over the two datasets, we utilised

474 the HALLMARK gene sets that encompass 50 distinct biological processes (rather than the
475 186 KEGG gene sets that share many genes).

476 The latent variables estimated by AES-PCA for the HALLMARK gene sets (i.e. the first
477 principal components) in each dataset did not show any significant association with *psen1*
478 genotype, suggesting that changes to gene expression (measured over entire brains) are too
479 subtle to be detected as statistically significant using this method. However, clustering of the
480 calculated PC1 values by AES-PCA for each HALLMARK gene set in each sample and dataset
481 revealed that samples in the Q96_K97del dataset clustered mostly according to genotype
482 (one wild type sample did not follow the trend), supporting that heterozygosity for the
483 Q96_K97del mutation does result in marked effects on gene expression for the HALLMARK
484 gene sets. Conversely, clustering of PC1 values in the T428del dataset resulted in two distinct
485 clusters of samples. However, samples did not group by genotype over the two clusters to
486 the same extent as seen for the Q96_K97del dataset. Intriguingly, the Q96_K97del dataset
487 had less sample numbers per genotype (n = 4), and did not have as great sequencing depth
488 as the current RNA-seq experiment. Therefore, this supports that heterozygosity for the
489 Q96_K97del mutation has more consistent (more severe) effects on young adult brain
490 transcriptomes than heterozygosity for the T428del mutation (**Figure 7 B,C**).

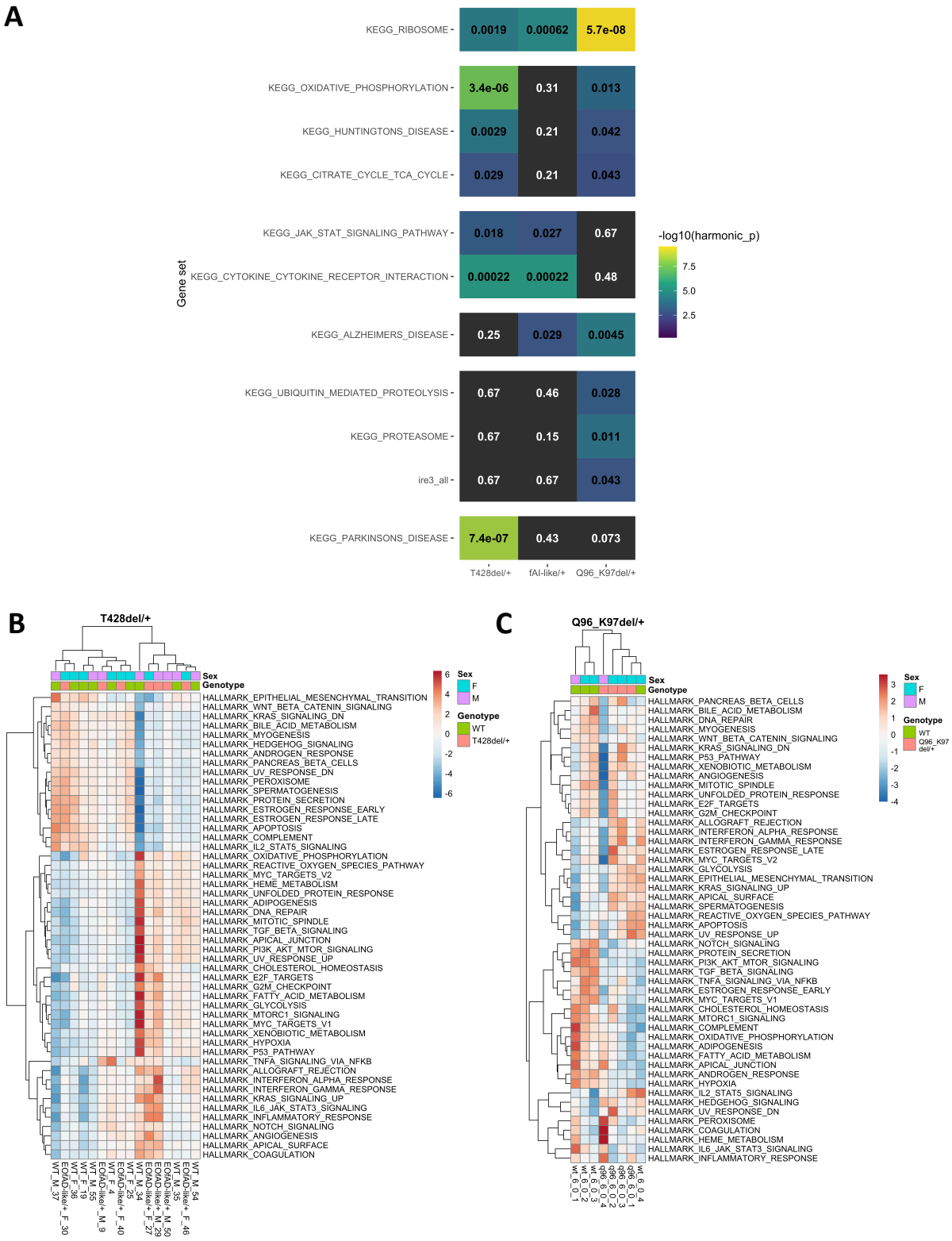
A
Gene set
KEGG_RIBOSOME
KEGG_OXIDATIVE_PHOSPHORYLATION
KEGG_HUNTINGTONS_DISEASE
KEGG_CITRATE_CYCLE_TCA_CYCLE
KEGG_JAK_STAT_SIGNALING_PATHWAY
KEGG_CYTOKINE_CYTOKINE_RECEPTOR_INTERACTION
KEGG_ALZHEIMERS_DISEASE
KEGG_UBIQUITIN_MEDIATED_PROTEOLYSIS
KEGG_PROTEASOME
ire3_all
KEGG_PARKINSONS_DISEASE
T428del/+
fAl-like/+
Q96_K97del/+
-log10(harmonic_p)
B
T428del/+
Sex
Genotype
C
Q96_K97del/+

492 **Figure 7: A** Comparison of KEGG and IRE gene sets significantly altered by the EOfAD-like mutations T428del and
493 Q96_K97del in 6-month-old zebrafish brains. Each cell is coloured according to statistical significance, and the FDR-adjusted
494 harmonic mean p-value is shown. Gene sets not significantly altered (FDR adjusted harmonic mean p-value > 0.05) in a
495 comparison between a *psen1* mutant zebrafish with their respective wild type siblings appear grey. **B** Principal component 1
496 (PC1) values for the HALLMARK gene sets as calculated by AES-PCA, clustered based on their Euclidean distance in
497 T428del/+ samples relative to their wild type siblings. **C** PC1 values for the HALLMARK gene sets as calculated by AES-PCA
498 clustered based on their Euclidean distance in Q96_K97del/+ samples relative to their wild type siblings at 6 months of age
499 under normal oxygen conditions.

500

501 ## DISCUSSION

502 In this study, we exploited transcriptome analysis of whole brains of young adult zebrafish
503 siblings, to detect differences in molecular state between the brains of fish heterozygous for
504 an EOfAD-like mutation or an fAI-like mutation of *psen1* compared to wild type *in vivo*. The
505 subtlety of the effects observed is consistent with that EOfAD is, despite its designation as
506 "early-onset", a disease affecting people overwhelmingly at ages older than 30 years [86].
507 The person reported to carry the T440del mutation of *PSEN1* showed cognitive decline at 41
508 years [47]. (Overall, EOfAD mutations in *PSEN1* show a median survival to onset of 45 years
509 [86]). In contrast, at 6 months of age, zebrafish are only recently sexually mature.
510 Nevertheless, since AD is thought to take decades to develop [32], it is these subtle, early
511 changes that we must target therapeutically if we wish to arrest the pathological processes
512 driving the progression to AD. As seen in all our previous analyses of EOfAD-like mutations
513 [39-41, 43, 45], changes in expression of genes involved in oxidative phosphorylation were
514 identified as significant. However, this was not the case for the fAI-like, frameshift mutation.
515 Therefore, oxidative phosphorylation changes appear to be an early signature cellular stress
516 of EOfAD. Changes to mitochondrial function have been observed in heterozygous *PSEN1*
517 mutant astrocytes [87], homozygous *PSEN1* mutant neurons [88], and in neurons
518 differentiated from human induced pluripotent stem cells (hIPSCs) from sporadic AD
519 patients [89], supporting our findings. However, such changes are not always observed [90],
520 possibly due to issues of experimental reproducibility between laboratories when working
521 with hIPSCs [91].

522 The EOfAD-like mutation also caused very statistically significant changes in the
523 *KEGG_PARKINSONS_DISEASE* gene set (that shares many genes with
524 *KEGG_OXIDATIVE_PHOSPHORYLATION*) and the person carrying the *PSEN1*^{T440del} mutation
525 modelled by zebrafish *psen1*^{T428del} initially showed symptoms of early onset parkinsonism at
526 34 years of age before those of cognitive decline at 41 years [47].

527 In contrast to this EOfAD-like mutation, the fAI-like mutation apparently caused very
528 statistically significant changes in Notch signalling and changes in other signal transduction
529 pathways such as those involving Wnt and neurotrophins, as might be expected from
530 changes in γ-secretase activity. Also notable was enrichment for the
531 *KEGG_TOLL_LIKE_RECEPTOR_SIGNALLING_PATHWAY* gene set since acne inversa is a chronic
532 inflammatory skin disorder and, in humans, increased expression of Toll-like receptor 2 has
533 been noted in acne inversa lesions [92].

534 Both the EOfAD-like and fAI-like mutations caused very statistically significant changes in the
535 gene sets *KEGG_CYTOKINE_CYTOKINE_RECEPTOR _INTERACTION* and *KEGG_RIBOSOME*. The
536 former gene set reflects that both mutations appear to affect inflammation that is a
537 characteristic of the pathologies of both EOfAD [93] and fAI (reviewed in [94]). Like oxidative
538 phosphorylation, we have also observed effects on ribosomal protein genes sets for every
539 EOfAD-like mutation we have studied [39-41, 43]. This may be due protein synthesis
540 consuming a large proportion of cells' energy budgets [95] and requiring amino acid
541 precursors that can be sourced from lysosomes. Recently, Bordi et al [96] noted that mTOR
542 is highly activated in fibroblasts from people with Down syndrome (DS, trisomy 21). DS
543 individuals commonly develop EOfAD due to overexpression of the AβPP gene (that is

544 resident on human chromosome 21). The consequent increased expression of AβPP's β-
545 CTF/C99 fragment (generated by β-secretase cleavage of AβPP without γ-secretase cleavage)
546 affects endolysosomal pathway acidification [97] in a similar manner to EOfAD mutations of
547 *PSEN1* [98]. The mTOR protein is localised at lysosomes in the mTORC1 and mTORC2 protein
548 complexes (reviewed in [99, 100]) and monitors the energy and nutrient status of cells
549 (reviewed in [101]). It is important for regulating ribosomal activity, partly by regulating
550 transcription of ribosome components (reviewed in [102, 103]). Therefore, one explanation
551 for the consistent enrichment for transcripts of the *KEGG_RIBOSOME* gene set we see in
552 EOfAD mutant brains may be mTOR activation due to effects on lysosomal acidification
553 and/or the energy status of cells. We did not observe any significant changes to the
554 expression of genes involved in the mTOR signalling pathway in the analyses described in
555 this paper (the FDR-adjusted harmonic mean p-value for the
556 *KEGG_MTOR_SIGNALING_PATHWAY* was 0.7 for each comparison of the *psen1* mutant fish
557 to their wild type siblings, see **Supplementary Table 2**). However, these changes could be
558 undetectably subtle in young adult brains and/or occurring at the protein level and therefore
559 not observable in bulk RNA-seq data. (Statistically significant enrichment for genes in the
560 *HALLMARK_PI3K_AKT_MTOR_SIGNALING* gene set was seen previously for the normoxic, 6-
561 month-old brains of fish heterozygous for the more severe EOfAD-like mutation Q96_K97del
562 when compared to wild type siblings [45].)

563 While the brain transcriptome alterations caused by the EOfAD-like and fAI-like mutations
564 are subtle (as illustrated by the lack of tight clustering of samples in the principal component
565 analysis in **Figure 3,** and the low number of significantly differentially expressed genes), we
566 are reassured in their overall veracity by their similarity to the results of a parallel analysis of

567 sibling brain transcriptomes from 6-month-old zebrafish heterozygous for either a frameshift
568 or a frame-preserving mutation in the zebrafish *psen2* gene relative to wild type [40]. In that
569 similarly structured (but less statistically powered) experiment, only the frameshift mutation
570 significantly affected the *KEGG_NOTCH_SIGNALLING* gene set while only the frame-
571 preserving, EOfAD-like mutation significantly affected the
572 *KEGG_OXIDATIVE_PHOSPHORYLATION* gene set. Both *psen2* genotypes affected the
573 *KEGG_RIBOSOME* gene set, but in overall opposite directions (the frameshift mutation
574 largely upregulated these genes while the frame-preserving mutation did the opposite).

575 Transcriptome analysis can reveal a great deal of data on differences in gene transcript levels
576 between different genotypes or treatments. However, interpreting changes in cellular state
577 from this information is not straight forward. Are any changes seen direct molecular effects
578 of a mutation/treatment (e.g. the direct, downstream effects of a change in γ-secretase
579 activity) or homeostatic responses as cells/tissues adjust their internal states to promote
580 survival? For example, in the *KEGG_NOTCH_SIGNALING_PATHWAY* gene set shown in **Figure**
581 **6B**, more pathway components are upregulated than are downregulated. However, the
582 direct transcriptional targets of Notch signalling (*her4.2* and *heyl*) are downregulated, as
583 might be expected from reduced expression of wild type, catalytically-competent Psen1
584 protein. The upregulation of other components of the pathway may represent homeostatic
585 responses attempting to restore normal levels of Notch signalling.

586 Only two Notch downstream transcriptional target genes are described in the
587 *KEGG_NOTCH_SIGNALING_PATHWAY* gene set. Therefore, in an effort to assess more
588 generally the effects of the EOfAD-like and fAI-like mutations on γ-secretase activity, we also

589 analysed additional sets of genes previously identified (in various systems) as direct
590 transcriptional targets of γ-secretase-dependent signalling. One of these sets, encompassing
591 genes identified as Notch signalling targets by both γ-secretase inhibitor responses and
592 binding of the Notch intracellular domain to chromatin, revealed apparent upregulation of
593 Notch signalling in both the EOfAD-like and fAI-like heterozygous mutant brains relative to
594 wild type siblings. In both EOfAD-like/+ and fAI-like/+ mutant brains, the most highly ranked
595 genes in terms of differential expression tended to be upregulated (although some highly
596 ranked genes were downregulated in fAI-like/+ brains). The idea that putative low levels of a
597 form of Psen1 protein truncated in the third lumenal loop domain could increase Notch
598 signalling is not unexpected, as we previously observed an implied upregulation of Notch
599 signalling in zebrafish embryos with forced expression of the fAI-causative P242Lfs allele of
600 human *PSEN1* [104]. However, a widespread assumption within AD research is that EOfAD-
601 like mutations of *PSEN1* decrease γ-secretase cleavage of AβPP [105], possibly through a
602 dominant negative mechanism [21]. This assumption conflicts with the observation of Sun et
603 al. [15] that approximately 10% of the 138 EOfAD mutations of human *PSEN1* they studied
604 actually increased γ-secretase cleavage of AβPP's β-CTF/C99 fragment (in experiments
605 examining the activities of the mutant proteins in isolation from wild type protein). Zhou et
606 al. [106] also observed increased γ-secretase activity (cleavage of AβPP's β-CTF/C99
607 fragment) due to an EOfAD mutation of *PSEN1* (S365A, this replicated Sun et al.'s finding for
608 this mutation).

609 It is important to note that mutations of *PSEN1* need not cause similar effects on Notch and
610 AβPP cleavage [104, 107, 108]. The transmembrane domains of the Notch receptor and the
611 APP's C99 fragment have different conformations [109]. Therefore, changes in the

612 conformation of PSEN1 within γ-secretase due to a mutation may differentially affect Notch
613 and C99 cleavage. Indeed, in our previously mentioned study of forced expression of the
614 human *PSEN1*^{P242Lfs} allele in zebrafish embryos, increased apparent Notch signalling was
615 observed without change in AβPP processing [104]. Conversely, Zhang et al. [108] showed
616 that transgenic expression of an EOfAD mutation S169del in *PSEN1* under the control of the
617 *Thy1* brain specific promotor altered the processing of AβPP *in vivo* without affecting Notch
618 signalling. Notably, both of these studies did not use the *PSEN1* gene's own promoter to
619 express mutant forms of this gene, and so the effects seen may be distorted by gene/protein
620 over-expression.

621 Unfortunately, the direct transcriptional targets of the intracellular domain of AβPP (AICD)
622 have not been characterised to the same extent as those of NICD (reviewed in [110]). This
623 constrains transcriptome analysis for detection of differential effects on γ-secretase cleavage
624 of AβPP caused by the EOfAD-like and fAI-like mutations. Future work should include further
625 investigation of how these mutations effect γ-secretase cleavage of AβPP *in vivo.*

626 In conclusion, we have performed the first direct comparison of an EOfAD-like and a fAI-like
627 mutation of *presenilin 1* in an *in vivo* model. Both forms of mutation cause apparent changes
628 in inflammation, downregulate expression of genes encoding the components of the
629 ribosome subunits, and potentially affect *γ*-secretase activity as supported by altered
630 expression of Notch signalling pathway transcriptional target genes. We see that changes to
631 mitochondrial function are a specific, common characteristic of EOfAD-like mutations while
632 the fAI-like mutation specifically affects important signal transduction pathways. These

633 differential effects on brain transcriptomes give insight into how reading-frame preserving
634 mutations in *PSEN1* cause EOfAD while frameshift mutations do not.

635 CONFLICT OF INTEREST/DISCLOSURE STATEMENT

636 The authors have no financial or non-financial competing interests to declare.

637 ACKNOWLEDGEMENTS

638 The authors would like to thank Dr. Nhi Hin for providing the Q96_K97del gene expression
639 values and the zebrafish IRE gene sets. We also would like to thank Dr. Jimmy Breen for his
640 assistance with using the Nextflow pipeline. The authors thank Dr Giuseppe Verdile for
641 critical reading of the manuscript.

642 This work was supported with supercomputing resources provided by the Phoenix HPC
643 service at the University of Adelaide and by grants GNT1061006 and GNT1126422 from the
644 National Health and Medical Research Council of Australia (NHMRC). KB was supported by
645 an Australian Government Research Training Program Scholarship and by funds from the
646 Carthew Family Charity Trust. YD was supported by an Adelaide Graduate Research
647 Scholarship from the University of Adelaide. MN was supported by funds from the grants
648 listed above. ML is an academic employee of the University of Adelaide.

649

650 ## REFERENCES

651 [1] Janssen JC, Beck JA, Campbell TA, Dickinson A, Fox NC, Harvey RJ, Houlden H, Rossor
652 MN, Collinge J (2003) Early onset familial Alzheimer's disease: Mutation frequency in
653 31 families. *Neurology* **60**, 235-239.

654 [2] Żekanowski C, Styczyńska M, Pepłońska B, Gabryelewicz T, Religa D, Ilkowski J,
655 Kijanowska-Haładyna B, Kotapka-Minc S, Mikkelsen S, Pfeffer A, Barczak A, Łuczywek
656 E, Wasiak B, Chodakowska-Żebrowska M, Gustaw K, Łączkowski J, Sobów T, Kuźnicki
657 J, Barcikowska M (2003) Mutations in presenilin 1, presenilin 2 and amyloid precursor
658 protein genes in patients with early-onset Alzheimer's disease in Poland.
659 *Experimental Neurology* **184**, 991-996.

660 [3] Cruts M, van Duijn CM, Backhovens H, Van den Broeck M, Wehnert A, Serneels S,
661 Sherrington R, Hutton M, Hardy J, St George-Hyslop PH (1998) Estimation of the
662 genetic contribution of presenilin-1 and-2 mutations in a population-based study of
663 presenile Alzheimer disease. *Human molecular genetics* **7**, 43-51.

664 [4] Kamimura K, Tanahashi H, Yamanaka H, Takahashi K, Asada T, Tabira T (1998) Familial
665 Alzheimer's disease genes in Japanese. *Journal of the neurological sciences* **160**, 76-
666 81.

667 [5] Area-Gomez E, de Groof AJ, Boldogh I, Bird TD, Gibson GE, Koehler CM, Yu WH, Duff
668 KE, Yaffe MP, Pon LA, Schon EA (2009) Presenilins are enriched in endoplasmic
669 reticulum membranes associated with mitochondria. *American Journal of Pathology*
670 **175**, 1810-1816.

671 [6] Schon EA, Area-Gomez E (2010) Is Alzheimer's disease a disorder of mitochondria-
672 associated membranes? *J Alzheimers Dis* **20 Suppl 2**, S281-292.

673 [7] Laudon H, Hansson EM, Melén K, Bergman A, Farmery MR, Winblad B, Lendahl U, von
674 Heijne G, Näslund J (2005) A nine-transmembrane domain topology for presenilin 1. *J*
675 *Biol Chem* **280**, 35352-35360.

676 [8] Fukumori A, Fluhrer R, Steiner H, Haass C (2010) Three-amino acid spacing of
677 presenilin endoproteolysis suggests a general stepwise cleavage of gamma-secretase-
678 mediated intramembrane proteolysis. *J Neurosci* **30**, 7853-7862.

679 [9] Sun L, Zhao L, Yang G, Yan C, Zhou R, Zhou X, Xie T, Zhao Y, Wu S, Li X, Shi Y (2015)
680 Structural basis of human γ-secretase assembly. *Proceedings of the National*
681 *Academy of Sciences* **112**, 6003.

682 [10] Wolfe MS (2020) Unraveling the complexity of γ-secretase. *Semin Cell Dev Biol* **105**,
683 3-11.

684 [11] Dermaut B, Kumar-Singh S, Engelborghs S, Theuns J, Rademakers R, Saerens J, Pickut
685 BA, Peeters K, van den Broeck M, Vennekens K, Claes S, Cruts M, Cras P, Martin JJ,
686 Van Broeckhoven C, De Deyn PP (2004) A novel presenilin 1 mutation associated with
687 Pick's disease but not beta-amyloid plaques. *Ann Neurol* **55**, 617-626.

688 [12] Li D, Parks SB, Kushner JD, Nauman D, Burgess D, Ludwigsen S, Partain J, Nixon RR,
689 Allen CN, Irwin RP, Jakobs PM, Litt M, Hershberger RE (2006) Mutations of presenilin
690 genes in dilated cardiomyopathy and heart failure. *Am J Hum Genet* **79**, 1030-1039.

691 [13] Wang B, Yang W, Wen W, Sun J, Su B, Liu B, Ma D, Lv D, Wen Y, Qu T, Chen M, Sun M,
692 Shen Y, Zhang X (2010) -Secretase Gene Mutations in Familial Acne Inversa. **330**,
693 1065-1065.

694 [14] Jiang H, Jayadev S, Lardelli M, Newman M (2018) A Review of the Familial Alzheimer's
695 Disease Locus PRESENILIN 2 and Its Relationship to PRESENILIN 1. *Journal of*
696 *Alzheimer's Disease* **66**, 1323-1339.

697 [15] Sun L, Zhou R, Yang G, Shi Y (2017) Analysis of 138 pathogenic mutations in
698 presenilin-1 on the in vitro production of Aβ42 and Aβ40 peptides by γ-secretase.
699 *Proceedings of the National Academy of Sciences* **114**, E476-E485.

700 [16] Szaruga M, Veugelen S, Benurwar M, Lismont S, Sepulveda-Falla D, Lleo A, Ryan NS,
701 Lashley T, Fox NC, Murayama S, Gijsen H, De Strooper B, Chávez-Gutiérrez L (2015)
702 Qualitative changes in human γ-secretase underlie familial Alzheimer's disease. *J Exp*
703 *Med* **212**, 2003-2013.

704 [17] De Strooper B (2007) Loss-of-function presenilin mutations in Alzheimer disease.
705 Talking Point on the role of presenilin mutations in Alzheimer disease. *EMBO Rep* **8**,
706 141-146.

707 [18] Jayne T, Newman M, Verdile G, Sutherland G, Munch G, Musgrave I, Moussavi Nik
708 SH, Lardelli M (2016) Evidence for and Against a Pathogenic Role of Reduced gamma-
709 Secretase Activity in Familial Alzheimer's Disease. *Journal of Alzheimer's Disease*.

710 [19] Wong TH, Seelaar H, Melhem S, Rozemuller AJM, van Swieten JC (2020) Genetic
711 screening in early-onset Alzheimer's disease identified three novel presenilin
712 mutations. *Neurobiology of aging* **86**, 201.e209-201.e214.

713 [20] Lee JH, McBrayer MK, Wolfe DM, Haslett LJ, Kumar A, Sato Y, Lie PP, Mohan P, Coffey
714 EE, Kompella U, Mitchell CH, Lloyd-Evans E, Nixon RA (2015) Presenilin 1 Maintains
715 Lysosomal Ca(2+) Homeostasis via TRPML1 by Regulating vATPase-Mediated
716 Lysosome Acidification. *Cell Report* **12**, 1430-1444.

717 [21] Heilig EA, Gutti U, Tai T, Shen J, Kelleher RJ, 3rd (2013) Trans-dominant negative
718 effects of pathogenic PSEN1 mutations on γ-secretase activity and Aβ production. *J*
719 *Neurosci* **33**, 11606-11617.

720 [22] Schroeter EH, Ilagan MXG, Brunkan AL, Hecimovic S, Li Y-m, Xu M, Lewis HD, Saxena
721 MT, De Strooper B, Coonrod A, Tomita T, Iwatsubo T, Moore CL, Goate A, Wolfe MS,
722 Shearman M, Kopan R (2003) A presenilin dimer at the core of the γ-secretase
723 enzyme: Insights from parallel analysis of Notch 1 and APP proteolysis. *Proceedings*
724 *of the National Academy of Sciences* **100**, 13075.

725 [23] Brautigam H, Moreno CL, Steele JW, Bogush A, Dickstein DL, Kwok JBJ, Schofield PR,
726 Thinakaran G, Mathews PM, Hof PR, Gandy S, Ehrlich ME (2015) Physiologically
727 generated presenilin 1 lacking exon 8 fails to rescue brain PS1−/− phenotype and
728 forms complexes with wildtype PS1 and nicastrin. *Scientific Reports* **5**, 17042.

729 [24] Li X, Dang S, Yan C, Gong X, Wang J, Shi Y (2013) Structure of a presenilin family
730 intramembrane aspartate protease. *Nature* **493**, 56-61.

731 [25] De Gasperi R, Sosa MAG, Dracheva S, Elder GA (2010) Presenilin-1 regulates induction
732 of hypoxia inducible factor-1α: altered activation by a mutation associated with
733 familial Alzheimer's disease. *Molecular Neurodegeneration* **5**, 38-38.

734 [26] Villa JC, Chiu D, Brandes AH, Escorcia FE, Villa CH, Maguire WF, Hu CJ, de Stanchina E,
735 Simon MC, Sisodia SS, Scheinberg DA, Li YM (2014) Nontranscriptional role of Hif-
736 1alpha in activation of gamma-secretase and notch signaling in breast cancer. *Cell*
737 *Replication* **8**, 1077-1092.

738 [27] Newman M, Nik HM, Sutherland GT, Hin N, Kim WS, Halliday GM, Jayadev S, Smith C,
739 Laird AS, Lucas CW, Kittipassorn T, Peet DJ, Lardelli M (2020) Accelerated loss of
740 hypoxia response in zebrafish with familial Alzheimer’s disease-like mutation of
741 presenilin 1. *Human Molecular Genetics* **29**, 2379-2394.

742 [28] Lane DJR, Merlot AM, Huang MLH, Bae DH, Jansson PJ, Sahni S, Kalinowski DS,
743 Richardson DR (2015) Cellular iron uptake, trafficking and metabolism: Key molecules
744 and mechanisms and their roles in disease. *Biochimica et Biophysica Acta (BBA) -*
745 *Molecular Cell Research* **1853**, 1130-1144.

746 [29] Güner G, Lichtenthaler SF (2020) The substrate repertoire of γ-secretase/presenilin.
747 *Seminars in Cell & Developmental Biology* **105**, 27-42.

748 [30] Thinakaran G, Harris CL, Ratovitski T, Davenport F, Slunt HH, Price DL, Borchelt DR,
749 Sisodia SS (1997) Evidence that levels of presenilins (PS1 and PS2) are coordinately
750 regulated by competition for limiting cellular factors. *J Biol Chem* **272**, 28415-28422.

751 [31] Berchtold NC, Sabbagh MN, Beach TG, Kim RC, Cribbs DH, Cotman CW (2014) Brain
752 gene expression patterns differentiate mild cognitive impairment from normal aged
753 and Alzheimer's disease. *Neurobiology of Aging* **35**, 1961-1972.

754 [32] Villemagne VL, Burnham S, Bourgeat P, Brown B, Ellis KA, Salvado O, Szoeke C,
755 Macaulay SL, Martins R, Maruff P, Ames D, Rowe CC, Masters CL (2013) Amyloid β
756 deposition, neurodegeneration, and cognitive decline in sporadic Alzheimer's
757 disease: a prospective cohort study. *The Lancet Neurology* **12**, 357-367.

758 [33] Foley AM, Ammar ZM, Lee RH, Mitchell CS (2015) Systematic review of the
759 relationship between amyloid-β levels and measures of transgenic mouse cognitive
760 deficit in Alzheimer's disease. *J Alzheimers Dis* **44**, 787-795.

761 [34] Hargis KE, Blalock EM (2017) Transcriptional signatures of brain aging and
762 Alzheimer’s disease: What are our rodent models telling us? *Behavioural Brain*
763 *Research* **322**, 311-328.

764 [35] Guo Q, Fu W, Sopher BL, Miller MW, Ware CB, Martin GM, Mattson MP (1999)
765 Increased vulnerability of hippocampal neurons to excitotoxic necrosis in presenilin-1
766 mutant knock-in mice. *Nat Med* **5**, 101-106.

767 [36] Kawasumi M, Chiba T, Yamada M, Miyamae-Kaneko M, Matsuoka M, Nakahara J,
768 Tomita T, Iwatsubo T, Kato S, Aiso S, Nishimoto I, Kouyama K (2004) Targeted
769 introduction of V642I mutation in amyloid precursor protein gene causes functional
770 abnormality resembling early stage of Alzheimer's disease in aged mice. *Eur J*
771 *Neurosci* **19**, 2826-2838.

772 [37] Xu J, Burgoyne PS, Arnold AP (2002) Sex differences in sex chromosome gene
773 expression in mouse brain. *Human Molecular Genetics* **11**, 1409-1419.

774 [38] Bundy JL, Vied C, Nowakowski RS (2017) Sex differences in the molecular signature of
775 the developing mouse hippocampus. *BMC Genomics* **18**, 237.

776 [39] Barthelson K, Pederson S, Newman M, Lardelli M (2020) Transcriptome analysis of a
777 protein-truncating mutation in sortilin-related receptor 1 associated with early-onset
778 familial Alzheimer's disease indicates effects on mitochondrial and ribosome function
779 in young-adult zebrafish brains. *bioRxiv*, 2020.2009.2003.282277.

780 [40] Barthelson K, Pederson SM, Newman M, Jiang H, Lardelli M (2020) Frameshift and
781 frame-preserving mutations in zebrafish presenilin 2 affect different cellular
782 functions in young adult brains. *bioRxiv*, 2020.2011.2021.392761.

783 [41] Barthelson K, Pederson SM, Newman M, Lardelli M (2020) Brain transcriptome
784 analysis reveals subtle effects on mitochondrial function and iron homeostasis of
785 mutations in the SORL1 gene implicated in early onset familial Alzheimer's disease.
786 *Molecular Brain* **13**, 142.

787 [42] Hin N, Newman M, Kaslin J, Douek AM, Lumsden A, Nik SHM, Dong Y, Zhou X-F,
788 Mañucat-Tan NB, Ludington A, Adelson DL, Pederson S, Lardelli M (2020) Accelerated
789 brain aging towards transcriptional inversion in a zebrafish model of the K115fs
790 mutation of human PSEN2. *PLOS ONE* **15**, e0227258.

791 [43] Jiang H, Pederson SM, Newman M, Dong Y, Barthelson K, Lardelli M (2020)
792 Transcriptome analysis indicates dominant effects on ribosome and mitochondrial
793 function of a premature termination codon mutation in the zebrafish gene psen2.
794 *PLOS ONE* **15**, e0232559.

795 [44] Dong Y, Newman M, Pederson S, Hin N, Lardelli M (2020) Transcriptome analyses of
796 7-day-old zebrafish larvae possessing a familial Alzheimer's disease-like mutation in
797 psen1 indicate effects on oxidative phosphorylation, mcm functions, and iron
798 homeostasis. *bioRxiv*, 2020.2005.2003.075424.

799 [45] Hin N, Newman M, Pederson SM, Lardelli MM (2020) Iron Responsive Element (IRE)-
800 mediated responses to iron dyshomeostasis in Alzheimer's disease. *bioRxiv*,
801 2020.2005.2001.071498.

802 [46] Newman M, Hin N, Pederson S, Lardelli M (2019) Brain transcriptome analysis of a
803 familial Alzheimer's disease-like mutation in the zebrafish presenilin 1 gene implies
804 effects on energy production. *Molecular Brain* **12**.

805 [47] Ishikawa A, Piao Y-S, Miyashita A, Kuwano R, Onodera O, Ohtake H, Suzuki M,
806 Nishizawa M, Takahashi H (2005) A mutant PSEN1 causes dementia with lewy bodies
807 and variant Alzheimer's disease. *Annals of Neurology* **57**, 429-434.

808 [48] Zhang Y, Zhang Z, Ge W (2018) An efficient platform for generating somatic point
809 mutations with germline transmission in the zebrafish by CRISPR/Cas9-mediated
810 gene editing. *J Biol Chem* **293**, 6611-6622.

811 [49] Prykhozhij SV, Fuller C, Steele SL, Veinotte CJ, Razaghi B, Robitaille JM, McMaster CR,
812 Shlien A, Malkin D, Berman JN (2018) Optimized knock-in of point mutations in
813 zebrafish using CRISPR/Cas9. *Nucleic Acids Research* **46**, e102-e102.

814 [50] Jiang H, Newman M, Lardelli M (2018) The zebrafish orthologue of familial
815 Alzheimer's disease gene PRESENILIN 2 is required for normal adult melanotic skin
816 pigmentation. *PLOS ONE* **13**, e0206155.

817 [51] Di Tommaso P, Chatzou M, Floden EW, Barja PP, Palumbo E, Notredame C (2017)
818 Nextflow enables reproducible computational workflows. *Nature Biotechnology* **35**,
819 316-319.

820 [52] Team RC (2019) R: A language and environment for statistical computing. *R*
821 *Foundation for Statistical Computing, Vienna, Austria*.

822 [53] Chen Y, Lun A, Smyth G (2016) From reads to genes to pathways: differential
823 expression analysis of RNA-Seq experiments using Rsubread and the edgeR quasi-
824 likelihood pipeline [version 2; peer review: 5 approved]. *F1000Research* **5**.

825 [54] Robinson MD, Oshlack A (2010) A scaling normalization method for differential
826 expression analysis of RNA-seq data. *Genome Biology* **11**, R25.

827 [55] McCarthy DJ, Chen Y, Smyth GK (2012) Differential expression analysis of multifactor
828 RNA-Seq experiments with respect to biological variation. *Nucleic Acids Research* **40**,
829 4288-4297.

830 [56] Robinson MD, McCarthy DJ, Smyth GK (2009) edgeR: a Bioconductor package for
831 differential expression analysis of digital gene expression data. *Bioinformatics* **26**,
832 139-140.

833 [57] Young MD, Wakefield MJ, Smyth GK, Oshlack A (2010) Gene ontology analysis for
834 RNA-seq: accounting for selection bias. *Genome Biology* **11**, R14.

835 [58] Wu D, Lim E, Vaillant F, Asselin-Labat M-L, Visvader JE, Smyth GK (2010) ROAST:
836 rotation gene set tests for complex microarray experiments. *Bioinformatics* **26**, 2176-
837 2182.

838 [59] Wu D, Smyth GK (2012) Camera: a competitive gene set test accounting for inter-
839 gene correlation. *Nucleic acids research* **40**, e133-e133.

840 [60] Sergushichev AA (2016) An algorithm for fast preranked gene set enrichment analysis
841 using cumulative statistic calculation. *bioRxiv*, 060012.

842 [61] Subramanian A, Tamayo P, Mootha VK, Mukherjee S, Ebert BL, Gillette MA, Paulovich
843 A, Pomeroy SL, Golub TR, Lander ES, Mesirov JP (2005) Gene set enrichment analysis:
844 A knowledge-based approach for interpreting genome-wide expression profiles.
845 *Proceedings of the National Academy of Sciences* **102**, 15545.

846 [62] Kanehisa M, Goto S (2000) KEGG: kyoto encyclopedia of genes and genomes. *Nucleic*
847 *acids research* **28**, 27-30.

848 [63] Liberzon A (2014) A description of the Molecular Signatures Database (MSigDB) Web
849 site. *Methods Mol Biol* **1150**, 153-160.

850 [64] Dolgalev I (2020), p. R package.

851 [65] Chen X (2011) Adaptive elastic-net sparse principal component analysis for pathway
852 association testing. *Statistical applications in genetics and molecular biology* **10**, 48.

853 [66] Odom GJ, Ban Y, Liu L, Sun X, Pico AR, Zhang B, Wang L, Chen X (2019) pathwayPCA:
854 an R package for integrative pathway analysis with modern PCA methodology and
855 gene selection. *bioRxiv*, 615435.

856 [67] Liberzon A, Birger C, Thorvaldsdóttir H, Ghandi M, Mesirov Jill P, Tamayo P (2015)
857 The Molecular Signatures Database Hallmark Gene Set Collection. *Cell Systems* **1**,
858 417-425.

859 [68] Kosik KS, Muñoz C, Lopez L, Arcila ML, García G, Madrigal L, Moreno S, Ríos Romenets
860 S, Lopez H, Gutierrez M, Langbaum JB, Cho W, Suliman S, Tariot PN, Ho C, Reiman
861 EM, Lopera F (2015) Homozygosity of the autosomal dominant Alzheimer disease
862 presenilin 1 E280A mutation. *Neurology* **84**, 206-208.

863 [69] Parker J, Mozaffar T, Messmore A, Deignan JL, Kimonis VE, Ringman JM (2019)
864 Homozygosity for the A431E mutation in PSEN1 presenting with a relatively
865 aggressive phenotype. *Neurosci Lett* **699**, 195-198.

866 [70] Sundvik M, Chen Y-C, Panula P (2013) Presenilin1 Regulates Histamine Neuron
867 Development and Behavior in Zebrafish, <em>Danio rerio</em&gt. *The*
868 *Journal of Neuroscience* **33**, 1589.

869 [71] Tambini MD, D'Adamio L (2020) Knock-in rats with homozygous PSEN1(L435F)
870 Alzheimer mutation are viable and show selective γ-secretase activity loss causing
871 low Aβ40/42 and high Aβ43. *J Biol Chem* **295**, 7442-7451.

872 [72] Xia D, Watanabe H, Wu B, Lee SH, Li Y, Tsvetkov E, Bolshakov VY, Shen J, Kelleher RJ,
873 3rd (2015) Presenilin-1 knockin mice reveal loss-of-function mechanism for familial
874 Alzheimer's disease. *Neuron* **85**, 967-981.

875 [73] Nickless A, Bailis JM, You Z (2017) Control of gene expression through the nonsense-
876 mediated RNA decay pathway. *Cell & Bioscience* **7**, 26.

877 [74] Alhamdoosh M, Law CW, Tian L, Sheridan JM, Ng M, Ritchie ME (2017) Easy and
878 efficient ensemble gene set testing with EGSEA. *F1000Research* **6**, 2010-2010.

879 [75] Wilson DJ (2019) The harmonic mean p-value for combining dependent tests.
880 *Proceedings of the National Academy of Sciences* **116**, 1195.

881 [76] Pan Y, Lin MH, Tian X, Cheng HT, Gridley T, Shen J, Kopan R (2004) gamma-secretase
882 functions through Notch signaling to maintain skin appendages but is not required
883 for their patterning or initial morphogenesis. *Dev Cell* **7**, 731-743.

884 [77] Blanpain C, Lowry WE, Pasolli HA, Fuchs E (2006) Canonical notch signaling functions
885 as a commitment switch in the epidermal lineage. *Genes Dev* **20**, 3022-3035.

886 [78] Kopan R, Ilagan MX (2009) The canonical Notch signaling pathway: unfolding the
887 activation mechanism. *Cell* **137**, 216-233.

888 [79] Nowell C, Radtke F (2013) Cutaneous Notch signaling in health and disease. *Cold*
889 *Spring Harbor perspectives in medicine* **3**, a017772-a017772.

890 [80] Nguyen B-C, Lefort K, Mandinova A, Antonini D, Devgan V, Della Gatta G, Koster MI,
891 Zhang Z, Wang J, di Vignano AT, Kitajewski J, Chiorino G, Roop DR, Missero C, Dotto

892 GP (2006) Cross-regulation between Notch and p63 in keratinocyte commitment to
893 differentiation. *Genes & Development* **20**, 1028-1042.

894 [81] Dohda T, Maljukova A, Liu L, Heyman M, Grandér D, Brodin D, Sangfelt O, Lendahl U
895 (2007) Notch signaling induces SKP2 expression and promotes reduction of p27Kip1
896 in T-cell acute lymphoblastic leukemia cell lines. *Exp Cell Res* **313**, 3141-3152.

897 [82] Ryan RJH, Petrovic J, Rausch DM, Zhou Y, Lareau CA, Kluk MJ, Christie AL, Lee WY,
898 Tarjan DR, Guo B, Donohue LKH, Gillespie SM, Nardi V, Hochberg EP, Blacklow SC,
899 Weinstock DM, Faryabi RB, Bernstein BE, Aster JC, Pear WS (2017) A B Cell Regulome
900 Links Notch to Downstream Oncogenic Pathways in Small B Cell Lymphomas. *Cell Rep*
901 **21**, 784-797.

902 [83] El-Brolosy MA, Kontarakis Z, Rossi A, Kuenne C, Günther S, Fukuda N, Kikhi K, Boezio
903 GLM, Takacs CM, Lai S-L, Fukuda R, Gerri C, Giraldez AJ, Stainier DYR (2019) Genetic
904 compensation triggered by mutant mRNA degradation. *Nature* **568**, 193-197.

905 [84] Rossi A, Kontarakis Z, Gerri C, Nolte H, Hölper S, Krüger M, Stainier DYR (2015)
906 Genetic compensation induced by deleterious mutations but not gene knockdowns.
907 *Nature* **524**, 230-233.

908 [85] Luo W, Pant G, Bhavnasi YK, Blanchard SG, Jr., Brouwer C (2017) Pathview Web: user
909 friendly pathway visualization and data integration. *Nucleic Acids Research* **45**, W501-
910 W508.

911 [86] Ryman DC, Acosta-Baena N, Aisen PS, Bird T, Danek A, Fox NC, Goate A, Frommelt P,
912 Ghetti B, Langbaum JBS, Lopera F, Martins R, Masters CL, Mayeux RP, McDade E,
913 Moreno S, Reiman EM, Ringman JM, Salloway S, Schofield PR, Sperling R, Tariot PN,
914 Xiong C, Morris JC, Bateman RJ (2014) Symptom onset in autosomal dominant
915 Alzheimer disease: A systematic review and meta-analysis. *Neurology* **83**, 253-260.

916 [87] Oksanen M, Petersen AJ, Naumenko N, Puttonen K, Lehtonen Š, Gubert Olivé M,
917 Shakirzyanova A, Leskelä S, Sarajärvi T, Viitanen M, Rinne JO, Hiltunen M, Haapasalo
918 A, Giniatullin R, Tavi P, Zhang S-C, Kanninen KM, Hämäläinen RH, Koistinaho J (2017)
919 PSEN1 Mutant iPSC-Derived Model Reveals Severe Astrocyte Pathology in
920 Alzheimer's Disease. *Stem Cell Reports* **9**, 1885-1897.

921 [88] Martín-Maestro P, Sproul A, Martinez H, Paquet D, Gerges M, Noggle S, Starkov AA
922 (2019) Autophagy Induction by Bexarotene Promotes Mitophagy in Presenilin 1
923 Familial Alzheimer’s Disease iPSC-Derived Neural Stem Cells. *Molecular Neurobiology*
924 **56**, 8220-8236.

925 [89] Birnbaum JH, Wanner D, Gietl AF, Saake A, Kündig TM, Hock C, Nitsch RM,
926 Tackenberg C (2018) Oxidative stress and altered mitochondrial protein expression in
927 the absence of amyloid-β and tau pathology in iPSC-derived neurons from sporadic
928 Alzheimer's disease patients. *Stem Cell Res* **27**, 121-130.

929 [90] Kwart D, Gregg A, Scheckel C, Murphy EA, Paquet D, Duffield M, Fak J, Olsen O,
930 Darnell RB, Tessier-Lavigne M (2019) A Large Panel of Isogenic APP and PSEN1
931 Mutant Human iPSC Neurons Reveals Shared Endosomal Abnormalities Mediated by
932 APP β-CTFs, Not Aβ. *Neuron* **104**, 256-270.e255.

933 [91] Volpato V, Smith J, Sandor C, Ried JS, Baud A, Handel A, Newey SE, Wessely F, Attar
934 M, Whiteley E, Chintawar S, Verheyen A, Barta T, Lako M, Armstrong L, Muschet C,
935 Artati A, Cusulin C, Christensen K, Patsch C, Sharma E, Nicod J, Brownjohn P, Stubbs
936 V, Heywood WE, Gissen P, De Filippis R, Janssen K, Reinhardt P, Adamski J, Royaux I,
937 Peeters PJ, Terstappen GC, Graf M, Livesey FJ, Akerman CJ, Mills K, Bowden R,
938 Nicholson G, Webber C, Cader MZ, Lakics V (2018) Reproducibility of Molecular
939 Phenotypes after Long-Term Differentiation to Human iPSC-Derived Neurons: A
940 Multi-Site Omics Study. *Stem Cell Reports* **11**, 897-911.

941 [92] Hunger RE, Surovy AM, Hassan AS, Braathen LR, Yawalkar N (2008) Toll-like receptor
942 2 is highly expressed in lesions of acne inversa and colocalizes with C-type lectin
943 receptor. *British Journal of Dermatology* **158**, 691-697.

944 [93] Otani K, Shichita T (2020) Cerebral sterile inflammation in neurodegenerative
945 diseases. *Inflammation and Regeneration* **40**, 28.

946 [94] Zouboulis CC, Benhadou F, Byrd AS, Chandran NS, Giamarellos-Bourboulis EJ,
947 Fabbrocini G, Frew JW, Fujita H, González-López MA, Guillem P, Gulliver WPF,
948 Hamzavi I, Hayran Y, Hórvath B, Hüe S, Hunger RE, Ingram JR, Jemec GBE, Ju Q,
949 Kimball AB, Kirby JS, Konstantinou MP, Lowes MA, MacLeod AS, Martorell A,
950 Marzano AV, Matusiak Ł, Nassif A, Nikiphorou E, Nikolakis G, Nogueira da Costa A,
951 Okun MM, Orenstein LAV, Pascual JC, Paus R, Perin B, Prens EP, Röhn TA, Szegedi A,
952 Szepietowski JC, Tzellos T, Wang B, van der Zee HH (2020) What causes hidradenitis
953 suppurativa ?—15 years after. *Experimental Dermatology* **29**, 1154-1170.

954 [95] Research IoMUCoMN (1999) The Energy Costs of Protein Metabolism: Lean and
955 Mean on Uncle Sam's Team In *The Role of Protein and Amino Acids in Sustaining and*
956 *Enhancing Performance* National Academies Press (US), Washington (DC).

957 [96] Bordi M, Darji S, Sato Y, Mellén M, Berg MJ, Kumar A, Jiang Y, Nixon RA (2019) mTOR
958 hyperactivation in Down Syndrome underlies deficits in autophagy induction,
959 autophagosome formation, and mitophagy. *Cell Death & Disease* **10**, 563.

960 [97] Jiang Y, Sato Y, Im E, Berg M, Bordi M, Darji S, Kumar A, Mohan PS, Bandyopadhyay
961 U, Diaz A, Cuervo AM, Nixon RA (2019) Lysosomal Dysfunction in Down Syndrome Is
962 APP-Dependent and Mediated by APP-βCTF (C99). *The Journal of Neuroscience* **39**,
963 5255.

964 [98] Lee JH, Yu WH, Kumar A, Lee S, Mohan PS, Peterhoff CM, Wolfe DM, Martinez-
965 Vicente M, Massey AC, Sovak G, Uchiyama Y, Westaway D, Cuervo AM, Nixon RA
966 (2010) Lysosomal proteolysis and autophagy require presenilin 1 and are disrupted
967 by Alzheimer-related PS1 mutations. *Cell* **141**, 1146-1158.

968 [99] Linke M, Fritsch SD, Sukhbaatar N, Hengstschläger M, Weichhart T (2017) mTORC1
969 and mTORC2 as regulators of cell metabolism in immunity. *FEBS letters* **591**, 3089-
970 3103.

971 [100] Inpanathan S, Botelho RJ (2019) The Lysosome Signaling Platform: Adapting With the
972 Times. *Frontiers in Cell and Developmental Biology* **7**, 113.

973 [101] Bond P (2016) Regulation of mTORC1 by growth factors, energy status, amino acids
974 and mechanical stimuli at a glance. *J Int Soc Sports Nutr* **13**, 8.

975 [102] Loewith R, Hall MN (2011) Target of rapamycin (TOR) in nutrient signaling and growth
976 control. *Genetics* **189**, 1177-1201.

977 [103] Lempiäinen H, Shore D (2009) Growth control and ribosome biogenesis. *Current*
978 *Opinion in Cell Biology* **21**, 855-863.

979 [104] Newman M, Wilson L, Verdile G, Lim A, Khan I, Moussavi Nik SH, Pursglove S,
980 Chapman G, Martins RN, Lardelli M (2014) Differential, dominant activation and
981 inhibition of Notch signalling and APP cleavage by truncations of PSEN1 in human
982 disease. *Human Molecular Genetics* **23**, 602-617.

983 [105] Kelleher RJ, Shen J (2017) Presenilin-1 mutations and Alzheimer's disease.
984 *Proceedings of the National Academy of Sciences* **114**, 629.

985 [106] Zhou R, Yang G, Shi Y (2017) Dominant negative effect of the loss-of-function γ-
986 secretase mutants on the wild-type enzyme through heterooligomerization. *Proc Natl*
987 *Acad Sci U S A* **114**, 12731-12736.

988 [107] Chávez-Gutiérrez L, Bammens L, Benilova I, Vandersteen A, Benurwar M, Borgers M,
989 Lismont S, Zhou L, Van Cleynenbreugel S, Esselmann H, Wiltfang J, Serneels L, Karran
990 E, Gijsen H, Schymkowitz J, Rousseau F, Broersen K, De Strooper B (2012) The

991 mechanism of γ-Secretase dysfunction in familial Alzheimer disease. *The EMBO*
992 *Journal* **31**, 2261-2274.

993 [108] Zhang S, Cai F, Wu Y, Bozorgmehr T, Wang Z, Zhang S, Huang D, Guo J, Shen L, Rankin
994 C, Tang B, Song W (2020) A presenilin-1 mutation causes Alzheimer disease without
995 affecting Notch signaling. *Molecular Psychiatry* **25**, 603-613.

996 [109] Deatherage CL, Lu Z, Kroncke BM, Ma S, Smith JA, Voehler MW, McFeeters RL,
997 Sanders CR (2017) Structural and biochemical differences between the Notch and the
998 amyloid precursor protein transmembrane domains. *Science Advances* **3**, e1602794.

999 [110] Bukhari H, Glotzbach A, Kolbe K, Leonhardt G, Loosse C, Müller T (2017) Small things
1000 matter: Implications of APP intracellular domain AICD nuclear signaling in the
1001 progression and pathogenesis of Alzheimer's disease. *Progress in Neurobiology* **156**,
1002 189-213.

1003